TU Delft

Offshore Engineering

Graduation Thesis

The Bubble Barrier

Author:
Lotte Spaargaren

Supervisors:
Prof.dr.ir. W.S.J. Uijttewaal
Dr. A. Jarquin Laguna
Ir. J.S. Hoving

June 4, 2018

*"Not everything that counts can be counted,
and not everything that can be counted counts."*

— Albert Einstein

Preface

I can be honest in the fact that I was not looking forward to do a graduation project after one and a half years of studying a lot more than surfing. My willingness to take action in favour of the environment and to spend my time out in nature was larger than my desire to sit in an office.

Until I figured out that my old friends Francis, Saskia and Anne Marieke from the sailing school started a project that was combining all my passions. The Great Bubble Barrier filters plastics from rivers, thereby reducing the amount of plastics entering the ocean. I immediately contacted them to investigate the possibilities to graduate on the project. Luckily, they were about as enthusiastic about the idea as I was. Before I had even found a professor we spend a month at Deltares exploring the possibilities of this concept.

With a lot of data, but without a research question, I went to the faculty to find a professor and supervisors. Right, this is not the right order of proceedings. Fortunately, Wim also got enthusiastic about the topic and decided to let me be his student. Soon also Antonio was involved, and things got rolling. Thanks to Otti's help and Ad's tolerance to Offshore students I even got the chance to sit at an office (who'd have thought?). Being surrounded by seriously studying and very fun people has made my life during this graduation project a lot better.

I want to thank Francis, Saskia and Anne Marieke for letting me be part of The Great Bubble Barrier. And of course Philip for the great times in the rubber boat. I want to thank my professor Wim, for letting me work on this outstanding project. I want to thank Antonio and Jeroen for helping me not just during this graduation, but all throughout my masters. I want to thank Ad and Otti for the desk I could use, and Marysa for all the paperwork. Thanks Sabine, Alejandra, Silke, Sotiria, Steffie, Carine, Floris, Gal, Selina, Maartje, Jochem, Juan and Said for the good times, coffee and lunch. Lastly, I want to thank Luuk, my parents and my sister, they are always there for me even when I'm unbearable to be with.

Abstract

Plastic pollution of our oceans is becoming a bigger problem every day. The production of new plastics is extremely cheap and convenient resulting in a lack of incentive to retrieve plastic litter. Annually 8 billion kg of plastics enter the ocean polluting the ocean environment, of which the largest part via rivers and other waterways. Eventually, plastic enters the food chain through fish and other sea life. Organisations are arising worldwide to reduce the plastic stream to the ocean. The Great Bubble Barrier is based on the idea of filtering plastics from rivers by making use of a bubble curtain.

The principle behind this idea is as follows: a long tube is placed diagonally across a river and air is pumped through it creating a wall of bubbles. The rising bubbles enhance upward entrainment of the surrounding water. When approaching the surface the vertical flow is transferred into horizontal flow away from the bubble curtain on both sides. Together with the crossflow, this horizontal flow induced by the bubbles drives the plastic to the side. This horizontal flow is strongest at the surface and decays linearly down to 25% of the water depth. Therefore, only the plastic litter floating in the upper layer is affected. The vertical and horizontal flow induced by the bubble curtain in still water has been extensively researched in the last century. In this thesis, the influence of the crossflow on the behaviour of the bubble curtain is explored. Predictions of the horizontal surface flow are based on a theoretical model and validated with experiments performed at the Eastern Scheldt Flume at Deltares.

The model is based on the assumption that the maximum bubble-induced horizontal velocity is not influenced by the strength of the crossflow. At every depth in the surface layer, the two velocities can be summed up. Depending on their magnitude and the angle of the curtain, the direction of the resulting flow at that depth can be calculated. If the resulting flow is directed to the upstream side of the bubble barrier, the plastics are assumed to stay on the upstream side too and will, therefore, be led to the side of the river. If the resultant is directed to the downstream side of the bubble curtain the plastics are assumed to break through.

The vertical velocity of water in the plume, as well as the horizontal bubble-induced velocity, is calculated using two equations. One is derived from the momentum balance and the second is empirically found by Bulson. The results of both equations are compared with the experiments. For the vertical velocity, the momentum balance derived equation gives better results, whereas Bulson's equation gives a higher accuracy for the horizontal velocity. The crossflow is described by a logarithmic profile.

For all angles and crossflow velocities, the airflow required to keep the resultant upstream can be calculated at every depth in the surface layer. The airflow that is theoretically required to keep the resultant at a 10 cm depth upstream, is shown to be sufficient to block 90% of the tested objects in all experimental setups. The smaller the angle relative to the direction of the crossflow, the smaller the total required airflow over the whole tube despite the longer required tube length.

This work has gained a better understanding of the working principle of a bubble curtain as a plastic barrier. Further research on its performance in deeper waters is advised.

Contents

List of Tables

List of Figures

Symbols

A_{bubble} Cross sectional area of the rising bubble [m^2].

A Cross sectional area of the flow [m^2].

$B(z)$ Buoyancy force per meter from depth of tube to cross section z [N/m].

B_0 Initial buoyancy flux [m^3/s^3].

D_{bubble} Diameter of the rising bubble [m^2].

H_0 Atmospheric pressure expressed as a head of water [m].

H Head of water above the tube [m].

$M_z(z)$ Vertical momentum flux per meter width at cross section z [N/m].

M_{x0} Horizontal momentum flux per meter width of horizontal surface flow right after the impingement zone, on one side [N/m].

M_{z0} Initial vertical momentum flux per meter at release of bubbles from tube [N/m].

P Wetted perimeter [m].

Q_t Volume of air delivered by the compressor at atmospheric pressure for the whole tube. In normal litres per minute, this is the unit that was measured at Deltares. 1 m^3/s = 1 Nl/min / 60000 [Nl/min].

Q_0 Volume flux per unit length at depth of the tube [m^2/s].

Q_{atm} Volume flux per unit length at atmospheric pressure [m^2/s].

Q Volume of the bubble discharge per unit length [m^2/s].

Re Reynolds Number, low-laminar high-turbulent.

R Hydraulic radius [m].

V_{bubble} Volume of the rising bubble [m^3].

$\Delta\rho(x, z)$ Density defect at location (x,z) [kg/m^3].

$\Delta\rho_m(z)$ Density defect at centreline at height z above the tube [kg/m^3].

α Ratio between spreading of bubbles and water plume.

δ Angle of the resultant of the horizontal bubble induced velocity and the crossflow, relative to the direction of the crossflow [°].

$\dot{m}_0$ Mass discharge rate per unit length at the depth of the tube [kg/ms].

$\dot{m}(z)$ Mass flux at height z [kg/ms].

κ Von Kármán's constant.

μ_w Dynamic viscosity of water [kg/ms].

ϕ Angle of the tube relative to the direction of the crossflow [°].

ρ_a^0 Density of air at depth of the tube [kg/m³].

ρ_a^{atm} Density of air under atmospheric pressure [kg/m³].

ρ_a^z Density of air at height z [kg/m³].

$\rho_m(x,z)$ Density of water-air mixture at location (x,z) [kg/m³].

ρ_w Density of ambient water [kg/m³].

σ Standard deviation of the Gaussian distribution.

τ_b Bottom shear stress [Pa].

c_d Discharge coefficient.

c_{drag} Drag coefficient of a rising bubble.

c_f Friction coefficient calculated with Colebrook White.

c Spreading ratio.

$f_{buoyancy}$ Buoyancy force acting on a rising bubble [N].

f_{drag} Drag force acting on a rising bubble [N].

g Gravitational acceleration [m/s²].

h_s Critical height above source at which separation occurs [m].

p_0 Pressure at the depth of the tube [Pa].

p_{atm} Atmospheric pressure [Pa].

s Slope of the river.

t_c Characteristic time [s].

u_m Maximum surface velocity induced by the bubble curtain [m/s].

u_* Friction velocity [m/s].

u_{avg} Averaged velocity over depth [m/s].

u_{cr} Velocity of the crossflow in x-direction [m/s].

u_{log} Logarithmic velocity profile [m/s].

$w(x, z)$ Vertical velocity of the plume at location (x,z) [m/s].

w_0 Bubble discharge velocity [m/s].

w_b Bubble slip velocity [m/s].

w_m Maximum vertical velocity in the middle of the rising column [m/s].

w_{mean} Mean rising velocity of the plume [m/s].

z_0 Location of analytical origin below tube [m].

z_{imp} Height of the bottom of the impingement zone above tube [m].

z_{rough} Roughness length [m].

z Vertical distance above tube [m].

Chapter 1

Introduction

In this chapter, an introduction to plastics is given. First, the resources and properties are discussed. Then the negative influences of plastic on the environment are addressed, followed by an overview of the solutions to this problem. Finally, the subject of this research is explained, as well as the research goal, sub-questions and the approach.

1.1 Background of plastics

The demand for manufactured goods and packaging has increased drastically since the 1950s. Due to its stunning durability and very low costs, plastics have become the obvious choice in many situations. For many centuries society has used the ocean as a convenient place to dispose waste products, either intentionally or by accident. The low costs of new plastics make it uninviting to retain the value of post-use plastics. In the absence of adequate action to process post-use plastics, the amazing property of plastic to sustain has become a catastrophe for the ocean's environment. Annually 8 million tonnes of plastics enter the oceans, of which 80% originates from the land, the rest is fishing and shipping litter. Subsequently 80% of this land-based plastic arrives in the ocean via rivers and other waterways from urban and agricultural areas, the rest via beaches [GESAMP, 2015].

Figure 1.1: Campaign of Surfrider Foundation (see section 1.3)[https://www.surfrider.org/]

Table 1.1: Main types of plastics with their abbreviation, annual production in million tonnes, specific gravity [Co, 1970] and the percentage of studies in which the type of plastics is found [Hidalgo-Ruz et al., 2012].

Name		Prod. [mt]	Specific gravity	Found [%]
Polyethylene	PE	14	0.91-0.97	79
Polypropylene	PP	9.2	0.90-0.91	64
Polyvinyl chloride	PVC	4.9	1.35-1.45	5
Polystyrene	PS	3.5	1.04-1.07	40
Polyurethane	PUR	3.5	0.02-0.2	2
Polyethylene terephthalate	PET	3.1	1.2-1.38	2
Polyamide (nylon)	PA	0.8	1.13-1.15	17

The term plastics is used to define a sub-category of the larger group of materials called polymers. Polymers are typically very large molecules with high molecular weights. To enhance the physical properties of the material additives can be added. These additives include fillers, plasticisers, colourants, stabilisers and processing aids.

Plastics are usually synthesised from fossil fuels, but they can also be derived from biomass. When a polymer is made from bio-based material is not necessarily biodegradable. If the polymer is, however, bio-degradable, it will only degrade under the right circumstances. One of the requirements for bio-degradation is a temperature over 65°C, in the ocean environment this is never reached. When bio-degradable plastics are collected for recycling together with regular petroleum-based plastics, they will have a negative influence on the quality of the recycled material.

There are many types of plastics, the dominating are listed in table 1.1. The percentage in the last column is the frequency of occurrence of the different polymers in 42 studies of microplastic debris samples at sea or in marine sediments listed by Hidalgo-Ruz [2012]. Note that types with higher densities like PVC and PET are found relatively little compared to their production. They do not necessarily end up in the natural environment less often, but they sink to the bottom and are therefore hard to find.

There are countless applications for which plastic is the obvious material choice. It is extremely cheap to produce. It has endless possible shapes and stiffnesses. A plastic bag is thin, transparent, flexible and durable. A garden chair is light, strong, water- and UV-resistant. Plastic suits itself for nearly all demands.

1.2 The Plastic Problem

An ever-increasing amount of produced plastic products are only used once. For example water bottles, plastic bags, coffee cups[1], food wraps[2], cutlery, plates, medical sterile wraps and cosmetic microbeads. Most often they are used for less than 10 minutes but they will sustain for hundreds of years.

Most types of plastic are recyclable. However, since types with variable melting temperatures are being collected together, the end product will not have the same stunning properties as its ingredients. Furthermore, the process of recycling is complicated and costly

---

[1]The 'cardboard' cups have a plastic coating, have you ever tried to put coffee in a cardboard box?
[2]Challenge: Go to a supermarket and leave without any plastics packaging.

Figure 1.2: Albatrosses confuse plastic for food because of the algae on the surface. Artwork by Chris Jordan[http://www.chrisjordan.com/gallery/midway/#CF000478%2019x25]

which results in higher prices than for new material. Altogether only a few percents of the produced plastic products consist of recycled material.

A large part of the plastic waste is burned and another large part ends up in landfills. The last part of the plastic waste, mostly packaging, ends up in the environment. This can either be intentionally; thrown out of the car, left after a picnic or thrown cigarette buts. Or unintentionally; overfull trash bins, taken by the wind or flushed in the shower or through the sink. A large part of this litter, especially light pieces end up in waterways and are taken downstream with the flow. Over time plastic debris deteriorates with or without the help of UV-radiation and mechanical forces like waves. The small pieces that are formed are called microplastics. They will continue to become smaller, but they will sustain. There are also first-hand microplastics, for example in scrub products.

Annually 322 million tonnes of plastics are produced, 8 million tonnes end up in the ocean[3,4].

The ocean is the source of 97% of our water and 50 to 70% of our oxygen. It regulates the climate, absorbs carbon dioxide and provides protein for more than a billion people [GESAMP, 2015]. As human beings, we are very dependent on the ocean for our continuing existence. Plastic litter in the marine system has negative effects on social, economical, and ecological aspects. The social and economical aspect relates to the attractiveness of the polluted environment resulting in less tourism. The ecological aspect relates to animals such as invertebrates, fish and birds ingesting microplastics, see figure 1.2. Small microplastics can cross cell membranes an cause inflammation and cell damage. The incited damage on an organism depends amongst others on the number of particles, size, shape, surface properties, polymer composition and the duration of exposure. Consumption of filter-feeding invertebrates such as mussels or oysters seems to be the most common route of human exposure to microplastics. The maximum concentration has been found in wild mussel from the Dutch coast with 13.2 particles per gram wet weight [Anderson, 2013]. When a piece of plastic debris is floating in water, microorganisms, plants, algae or animals accumulate

---

[3][PlasticsEurope, 2016]

[4][http://web.unep.org/environmentassembly/estimated-8-million-tons-plastic-waste-enter-world%E2%80%99s-oceans-each-year-0]

Table 1.2: Steps can be made at different places in the chain.

Reduce	Retain	Reclaim	Recycle
- Create Awareness - Prevent more production - Bio-degradable	- Prevent loss from system - Improve waste system	- From the street - From rivers - From the beach - From the ocean	- Better Recycling - Expand deposit system

on the surface or inside the object. This effect is called biofouling. Biofouling affects the floating debris by protecting it from the UV radiation and by changing the density. This often enhances the particle to sink into layers beyond the surface. When landed in the ocean a floating piece of plastic is very hard to reclaim. Moreover, a piece that rolls over the ocean bed is, in the current state of technology, forever lost. The amount of plastics entering the ocean is increasing. The effects are very complex and hard to predict.

1.3 Solutions to plastic pollution

The amount of plastic littering the environment can be reduced in different locations of the plastic life cycle chain. An overview of this chain and the corresponding actions can be seen in figure 1.2. Organisations on many different scales are arising with the goal of keeping the oceans clean. A couple of them will be discussed below.

The Plastic Soup Foundation has the main priority of raising awareness about plastic pollution. They had a successful campaign 'Beat the Microbead' to stop the addition of microplastics in care products[5].
The Plastic Soup Surfer got his name when he kite-surfed along the whole Dutch coast on a board he made from plastic trash he found on the beach. This is one of the missions to raise awareness about the plastic pollution he has completed. His current mission is to get a deposit fee on small PET bottles, to raise awareness he paddled from the source of the river Rhine all the way to the sea on a stand-up paddle board, again made from plastic litter[6].
The Surfrider Foundation is dedicated to the protection and enjoyment of the world's ocean, waves and beaches through an activist network. Figure 1.1 shows the postcards of the campaign 'No break for trash' with which they have organised many beach cleanups[7].
Plastic Whale wants to raise awareness, but they mainly want to have cleaner waters. They take groups on board to fish for plastics in the canals of Amsterdam, see figure 1.3. Their sloops are made of the plastics that they caught[8].
Mr Trash Wheel is a system that can be put in a river, a physical barrier leads the floating debris to he side of the river where it is filtered out of the water with a big wheel[9].
The Ocean Cleanup tries to catch plastics that are already floating around in the ocean by making use of the oceanic gyres that transports the debris[10].
The most effective solution would be to stop or drastically reduce the production of new

---

[5][https://www.plasticsoupfoundation.org/]
[6][http://plasticsoupsurfer.org/]
[7][https://www.surfrider.org/]
[8][https://plasticwhalefoundation.com/]
[9][http://baltimorewaterfront.com/healthy-harbor/water-wheel/]
[10][https://www.theoceancleanup.com/]

Figure 1.3: Plastic Whale on an excursion in the canals of Amsterdam

plastics. The value of old material would increase and plastic would not be seen as trash anymore. Unfortunately, major changes like this happen very slowly in nowadays society. Powerful cooperates are more concerned about their profits than about the environment. Therefore solutions also need to be found further away from the source. Rivers are a big supplier of plastics for the oceans. Plastics do not spend years in rivers and have therefore not degraded or sunk yet. This makes them easier to recover. All together rivers are a very convenient location to block plastic from flowing into the ocean. The concept that is researched in this paper focuses on this.

1.4   The bubble barrier concept

The people behind The Great Bubble Barrier (TGBB) came up with the idea to limit the plastic supply to the ocean by filtering it out of rivers making use of a bubble curtain. A bubble curtain is realised by fixing a perforated tube on the bottom of a river and compressing air through it. The released air bubbles rise to the surface entraining ambient water, this constitutes a plume driven by the buoyancy of the bubbles. When reaching the surface layer the entrained water flows outward, away from the bubble screen, see figure 1.4a. Placing the tube at an angle relative to the normal of the river results in a deflected surface flow influencing the path of objects floating in the surface layer of the river, see figure 1.4b. Since the largest part of marine litter has a density smaller than water, when installed correctly, the bubble barrier is able to navigate this (semi-)floating plastic debris to the side of the river where it can be subtracted easily. This solution does not hinder ship or fish from passing.

A bubble curtain is not a new concept, in chapter 2 the former applications are discussed. This research focuses on the working principle of a bubble curtain in flowing water with the purpose of blocking plastic debris from passing, an application that has not been researched yet. Flume experiments have been performed at Deltares. In this report, the available theory on bubble curtains is combined and compared with the results from these flume experiments.

(a) Side View. The line of circles represent the path of the rising bubbles.

(b) Top View. The line of circles represents the line of the rising bubbles.
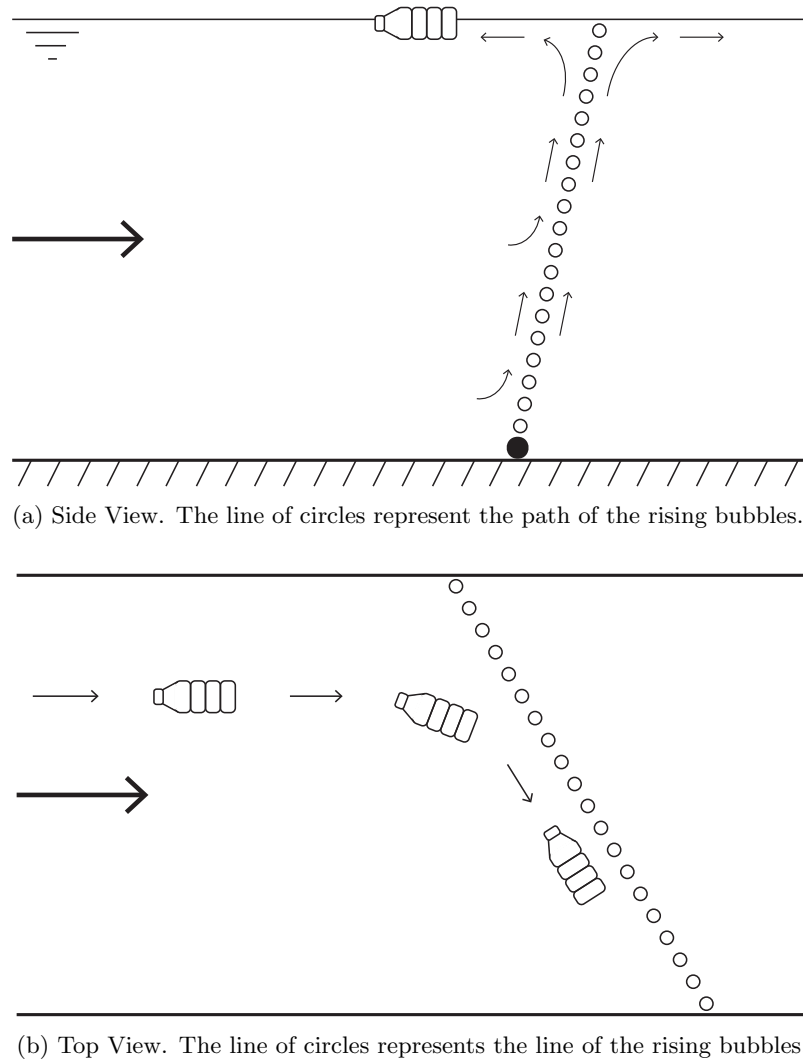
Figure 1.4: Schematics of the bubble barrier. The direction of the main flow is from left to right in both figures, indicated with the large arrow.

1.5 Research goal

The goal of this research is to get more insight in the working principle of the bubble barrier. One question is whether the available theory predicts the behaviour of the water around the bubble curtain in flowing water well. The limiting factors need to be found in order to design a bubble curtain that can redirect floating debris to the side. The research goal, therefore, is:

Optimise the concept of a bubble curtain to filter plastics from rivers.

1.6 Research questions

In order to reach the research goal. The following questions are answered in this report.

- What is the working principle of a bubble curtain in the function of a plastic filter?

- How does water approaching the bubble curtain behave?

- How does the plastic behave in the water?

- What variables are important to predict the working of the bubble barrier?

- How can the working of the bubble barrier on a small scale be predicted?

- Determine the required airflow to redirect plastic debris to the side.

1.7 Approach/Structure

This report will be structured as follows. Chapter 2 contains the literature study. The former work on bubble curtains is discussed together with phenomena important for this research. In chapter 3 an overview of the research is given. The theory with which the performance of the bubble curtain can be determined is presented. However, some values are missing that have to be determined from the experiments. The experimental setup and the method to obtain the data is given. In chapter 4 this data is gathered and a relation is sought to predict the values for other cases. The equations are filled in and the results are compared with the observations. Two theories are compared to see which one gives the most accurate predictions on the ability of the bubble curtain to redirect plastics to the side. Chapter 5 contains the discussion, conclusion and recommendations.

Chapter 2

Bubble curtain behaviour

In this chapter, the previously performed research on bubble curtains is presented. From this literature relations for the vertical velocity and the contained momentum of the plume are formed. The effect of the bubble curtain on the surface flow is investigated. Finally, the shape and influence of a crossflow are examined. Starting off with the general physics of an air bubble in water.

2.1 The rising of a bubble

When an air bubble is released underwater it rises to the surface. This phenomenon is enhanced by the density difference between water and air. The two main forces acting on the bubble are buoyancy and drag, see figure 2.1. The buoyancy of a bubble with volume V_{bubble} can be calculated as follows.

$$f_{buoyancy} = (\rho_w - \rho_a^z)V_{bubble}g \tag{2.1}$$

The surrounding water exerts a drag on the bubble. This drag force depends on the density of the surrounding fluid, the cross-sectional area A_{bubble} and the speed w_b of the bubble and the drag coefficient c_{drag}. The drag coefficient depends on the shape of the object and on the Reynolds Number.

$$f_{drag} = \frac{1}{2}\rho_w w_b^2 c_{drag} A_{bubble} \tag{2.2}$$

$$Re = \frac{w_b D_{bubble} \rho_w}{\mu_w} \tag{2.3}$$

As the bubble is rising the drag force enhances the surrounding water to be entrained upwards. In the case of a bubble curtain, many bubbles are rising closely together. Adjacent bubbles strongly influence each other and the flow becomes strongly turbulent. The previous equations do not describe this turbulent effect. In bubble curtain investigation it is advisable not to investigate the effect of single bubbles but to focus on the bigger picture. The entrained water constitutes a plume driven by the buoyancy of the bubbles. When reaching the surface layer the entrained water flows outward, away from the bubble screen creating a surface current.
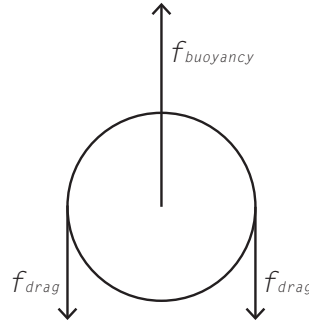
Figure 2.1: Forces acting on a rising bubble

2.2   Previous research on bubble curtains

In 1942 the idea arose that the surface current created by a bubble curtain might be able to function as a **wave breaker**. Sir Geoffrey Taylor [1955] did some calculations and found that when the current is directed against the incoming waves it should stop all waves shorter than a certain critical length. It was only in 1955 when Mr J. T. Evans [1955] performed experiments that Taylor's calculations were recovered and published.
Based on the theory of Schmidt [1941] for currents above a line source of heat, Taylor came up with the following empirical relation for the maximum vertical velocity on the middle of the rising column (w_m) depending on volume of the bubble discharge per unit length of the tube (Q) and the gravitational acceleration (g).

$$w_m = 1.9(Qg)^{1/3} \tag{2.4}$$

Abraham and Van der Burgh [1973] were the first ones to study bubble curtains to guard against saltwater intrusion into fresh water. This has been applied widely and is still functioning eg. in the 'Krammersluizen' in the South West of the Netherlands. From the 1970's bubble curtains have been evaluated as barriers in containing oil spills. This application has been used widely in the industry. Amongst others, Jen-Men Lo [1997] investigated the effect of wind, waves and currents in this application. He came up with a formula taking the effect of wind and current into account. He states that waves as big as 0.08 m with a period of 1.2s do not have a significant impact on the required airflow rate. Furthermore, bubble curtains are being used as underwater noise mitigation systems for offshore operations, to keep water around locks from freezing and to enrich inland waters with oxygen.

Air is compressible under pressure. The pressure under water increases with depth, every 10 meters 1 bar is added. When a 2 m long tube lays on the bottom of a 10 m deep river it, therefore, experiences twice the atmospheric pressure. If a volume flow of 1 m^3/s is delivered by the compressor, at the depth of the tube this will be compressed to 0.5 m^3/s. The length of the tube is variable, therefore the amount of delivered air is expressed per meter of the tube. In this case the volume flux per unit length at the depth of the tube Q_0=0.25 m^3/s, and the volume flux per unit length delivered by the compressor at atmospheric pressure $Q_{atm} = 0.5$ m^3/s. The relation between these two values takes the head of water H and the atmospheric pressure expressed as a head of water H_0 into account.
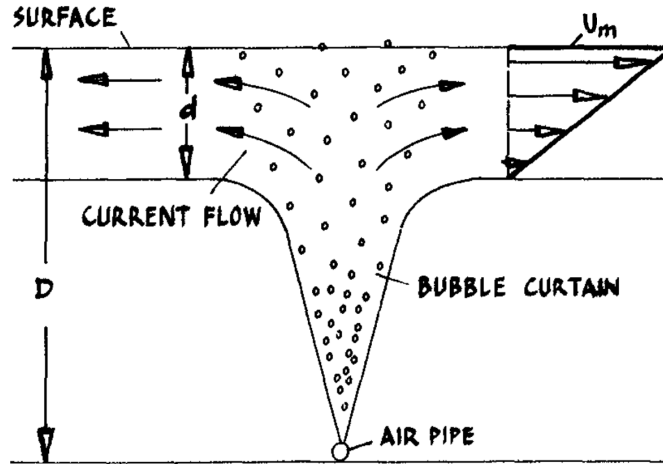
Figure 2.2: Schematisation of the bubble curtain. [Bulson, 1968]

$$Q_0 = \frac{H_0}{H_0 + H} Q_{atm} \tag{2.5}$$

Based on empirical measurements Bulson [1968] showed that the formula of Taylor (2.4), can be expressed in Q_{atm}, the quantity of free air delivered by the compressor per second per unit length. He performed large-scale experiments with water depths exceeding 10 meters. At a depth of 10 meters and an airflow of 5100 Nl/min/m, he found that the vertical velocity at the centre of the plume is about three-quarters of the horizontal surface velocity. Furthermore, he proved that the horizontal surface velocity is independent of the number of orifices and their diameters, as long as the same amount of air is being delivered. He came up with the following empirical formula for the maximum horizontal surface velocity (u_m), see figure 2.2.

$$u_m = k \left(\frac{gQ_{atm}H_0}{H + H_0} \right)^{1/3} \tag{2.6}$$

$$w_m = \frac{3}{4} u_m \tag{2.7}$$

In different pieces of literature, the factor k differs. However, since Bulson performed experiments on a scale comparable with rivers his value of k=1.46 is used in this study.

Fanneløp, Hirschberg and Küffer [1991] stated that for depths in access of 10-20 m the plume parameters can be assumed to be independent of depth since the speed of an air bubble in water (bubble slip velocity) is small in comparison with the plume velocity and a general solution can be obtained. The results from this similarity approach are approaching the numerical values a few metres above the source for plausible initial conditions. Since the waters in which the bubble curtain should operate will not always be deeper than 'a few meters' it is very important to work with the full numerical approach.

2.3   The rising plume

The initial momentum flux (M_{z0}) is given by the mass flow ($\dot{m}_0$) times the velocity(w_0). With a discharge coefficient (c_d) and the exit velocity of the air (w_0) is assumed to be loss-free. ρ_a^{atm} is the density of air at atmospheric pressure. The initial momentum flux per meter of tubing is given by the following formula. Where the volume flux (Q_{atm}) corresponds to the mass flux ($\dot{m}_0$) at atmospheric pressure.

$$M_{z0} = \dot{m}_0 w_0 = c_d w_0 \rho_a^{atm} Q_{atm} \tag{2.8}$$

$$\dot{m}_0 = \rho_a^{atm} Q_{atm} = \rho_a^0 Q_0 \tag{2.9}$$

The momentum flux increases with height due to the increasing buoyancy of the air contained in the bubbles. While leaving the tube, the air stream expands inversely proportional to the pressure drop over the orifice and breaks up into bubbles. The orifice diameter does not influence the bubble size, this only varies slightly with discharge rate [Kobus, 1968]. The bubbles in the plume vary in size but since the bubble slip velocity (w_b) only varies from 0.2-0.3 m/s with diameters ranging from 10^{-3} to 10^{-2} m [Ditmars and Cederwall, 1974] the assumption that w_b is equal to the terminal rise velocity of an air-bubble in stagnant water is appropriate. Milgram [1983] calculated the vertical centreline velocities of the plume with different values for w_b and found that a change of ± 0.05 m/s changes the centreline velocity by about 3%. Although the bubbles expand while moving upward, the rising speed can be considered independent of height. This because the speed of rising changes only little with the bubble diameter, which is proportional to the third root of the pressure difference. Therefore taking a constant value of 0.25 m/s for the bubble slip velocity should give suitable results.

The buoyant force of the air bubbles in a slice of water of thickness dz at height z ($dB(z)$) can be obtained by taking the product of the present air volume and the difference in specific weight between the ambient fluid and the air.

$$\rho_a^z = \frac{H_0 + H - z}{H_0} \rho_a^{atm} \tag{2.10}$$

$$dB(z) = \frac{\rho_a^{atm} Q_0 dz}{w_b} (\rho_w - \rho_a^z) g \tag{2.11}$$

Where ρ_a^z is the density of air at height z and ρ_w is the density of the ambient water. p_{atm} Is atmospheric pressure and p_0 is pressure at the depth of the tube.
Following the Boussinesq approximation $\rho_w - \rho_a^{atm} \approx \rho_w$ the buoyancy force up to height z is given by the following.

$$B(z) = \frac{p_{atm} Q_0}{w_b} \int_0^z \frac{dz}{H_0 + H - z} = \frac{p_{atm} Q_0}{w_b} \ln\left(1 - \frac{z}{H + H_0}\right) \tag{2.12}$$

The total momentum flux is the sum of the initial momentum and the buoyancy force.

$$M_z(z) = c_d w_0 \rho_a^{atm} Q_{atm} + \frac{p_{atm} Q_0}{w_b} \ln\left(1 - \frac{z}{H_0 + H}\right) \tag{2.13}$$

The buoyancy term grows rapidly going up from the tube and therefore the initial momentum term becomes negligible. Kobus [1968] shows that beyond 10% of the depth, the initial

momentum flux is less than 2% of the total momentum flux. Therefore an approximation of the momentum flux above the initial region is given by the buoyancy flux.

$$M_z(z) \approx \frac{p_{atm}Q_0}{w_b} \ln\left(1 - \frac{z}{H_0 + H}\right) \tag{2.14}$$

The upward velocity profile of the plume, as well as the density difference, are assumed to be Gaussian. At every point, the upward velocity ($w(x,z)$) can be described as a fraction of the maximum centreline velocity (w_m) depending on the spreading ratio (c) and the distance to the analytical origin (z_0). This analytical origin does not correspond to the location of the tube since the initial phase does not behave linearly (see figure 2.3).

$$w(x, z) = w_m(z)\, e^{-x^2/2c^2(z+z_0)^2} \tag{2.15}$$

$$\sigma = c(z + z_0) \tag{2.16}$$

Where σ is the standard deviation of the Gaussian profile of the vertical velocity of the water in the plume. Similar as the vertical centreline velocity also the density defect can be described by a Gaussian profile.

$$\Delta\rho(x, z) = \Delta\rho_m(z)\, e^{-x^2/2\alpha^2 c^2(z+z_0)^2} \tag{2.17}$$

With a negligible variation in density between the water-air mixture and the ambient water [Kobus, 1968]. Integration over the assumed velocity profile gives the mass flux ($\dot{m}(z)$):

$$\dot{m}(z) = 2\int_0^\infty \rho_m(x,z)w(x,z)dx = 2w_m(z)\int_0^\infty e^{-x^2/2c^2(z+z_0)^2} = \sqrt{2\pi}\rho_w w_m(z)c(z + z_0) \tag{2.18}$$

And hence the momentum flux:

$$M_z(z) = 2\int_0^\infty \rho_m(x,z)w(x,z)^2 dx = \sqrt{\pi}\rho_w w_m^2(z)c(z + z_0) \tag{2.19}$$

By neglecting the pressure difference over the depth and combining the equations 2.14 and 2.19 the following relation for the centreline velocity can be obtained.

$$w_m(z) = \sqrt{\frac{-p_{atm}Q_0\ln(1 - \frac{z}{H_0+H})}{\sqrt{\pi}\rho_w w_b c(z + z_0)}} \tag{2.20}$$

The vertical flow velocities can be described by this expression for the velocity (assumed Gaussian). To do this only the location of the analytical origin (z_0) and the rate of spread (c) need to be determined by experiments. This is done in this research, the method is elaborated in section 3.3.
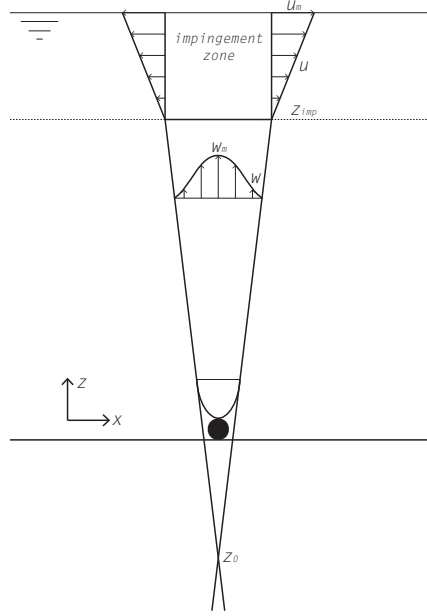
Figure 2.3: Side view from the bubble plume

2.4 Bubble-induced horizontal flow

Ditmars and Cederwall [1974] state that experiments indicate that above a line source of bubbles the region of horizontal flow is approximately 25% of the water depth and the flow has a linear decay in depth as shown in figure 2.3.

The maximum horizontal velocity induced by the bubbles (u_m) is described by Bulson in equation 2.6. Another way to get to this maximum velocity is by solving the momentum balance. The momentum flux of the horizontal surface flow on one side of the line of rising bubbles can be described as follows:

$$M_{x0} = \frac{0.25}{2} H \rho_w u_m^2 \tag{2.21}$$

Assuming that no momentum losses occur the maximum horizontal surface velocity can be defined by equating the vertical (equation 2.19) and the horizontal (equation 2.21) momentum around the impingement zone.

$$2M_{x0} = M_z(z_{imp}) \tag{2.22}$$

$$u_m = \sqrt{\frac{-p_{atm}Q_0 \ln(1 - \frac{z_{imp}}{H_0 + H})}{0.25 H \rho_w w_b}} \tag{2.23}$$

Away from the line of rising bubbles, the horizontal flow velocity decays linearly too. Right at the line of the rising bubbles, the horizontal velocity is at its maximum, at a horizontal distance of 4 times the water depth away from the line of rising bubbles the effect is zero [Riess and Fanneløp, 1998].
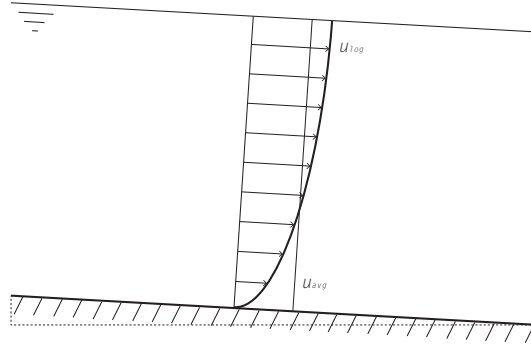
Figure 2.4: Logarithmic river profile.

2.5 The crossflow

The slope of the land between the mountain region and the ocean causes the water to flow down a river. In the mountains this slope is noticeable, closer to the ocean it decreases rapidly but the land remains sloping. The crossflow of the river deflects the plume in the downstream direction under an angle depending on the upward velocity of the mixture and the river flow velocity.

The crossflow is not constant over the vertical since near the bottom it experiences shear stress. The bottom shear stress (τ_b) depends on the density of the water (ρ_w), the gravitational acceleration (g), the hydraulic radius (R) and the slope of the waterway (s). Where the hydraulic radius is the cross-sectional area of the flow (A) divided by the wetted perimeter (P). The slope is calculated as the vertical distance over the horizontal distance. The shape of the crossflow is logarithmic and follows the following formulas.

$$\tau_b = \rho_w g R s = \rho_w g \frac{A}{P} s \tag{2.24}$$

To determine the shape of the profile, the roughness length (z_{rough}) and the Von Kármán's constant (κ) are used. The typical roughness length of a river is 0.05 m. The Von Kármán's constant has a universal value of 0.41 and is dimensionless. The friction velocity (u_*) has to be calculated first.

$$u_* = \sqrt{\frac{\tau_b}{\rho_w}} \tag{2.25}$$

$$u_{log} = \frac{u_*}{\kappa} \ln\left(\frac{z}{z_{rough}}\right) \tag{2.26}$$

The average flow velocity over the depth can be calculated using the following formula. The friction coefficient (c_f) is calculated with the Colebrook-White equation. [White, 2011]

$$u_{avg} = \sqrt{\frac{\tau_b}{\rho_w c_f}} \tag{2.27}$$

$$c_f = \left(\frac{\kappa}{\ln\left(\frac{30*0.37*R}{z_{rough}}\right)}\right)^2 \tag{2.28}$$
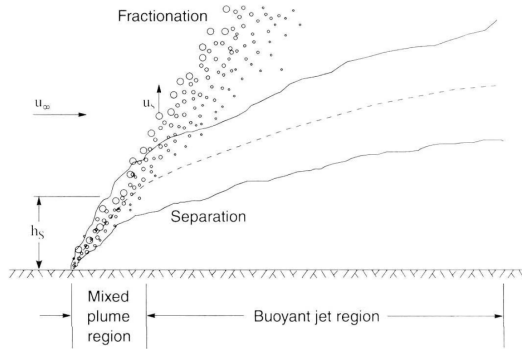
Figure 2.5: Definition sketch of the separation height and fractionation [Socolofsky and Adams, 2002].
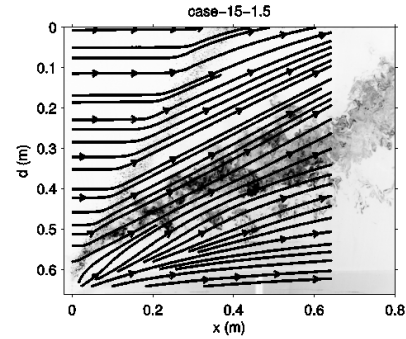
Figure 2.6: Planar Laser-Induced Fluorescence dye compared with Particle Image Velocimetry streamlines by Maryam Rezvani[2016].

2.6 Separation

In a mixed air-water plume, the air bubbles are not forced to follow the plume. Because of their buoyancy, they can slip relative to the plume. With a strong crossflow present, the entrained fluid can be pulled away from the rising bubbles. When the crossflow velocity exceeds the plume velocity on the downstream side of the plume, the crossflow pulls the fluid out of the plume. This phenomenon is called separation. Socolofsky and Adams [2002] described the critical height (h_s) at which separation occurs as a function of the initial buoyancy flux (B_0) based on their empirical research.

$$h_s = \frac{5.1 B_0}{(u_{cr} w_b^{2.4})^{0.88}} \tag{2.29}$$

$$B_0 = \frac{\Delta \rho}{\rho_w} Q_0 g \tag{2.30}$$

The weaker the crossflow and the larger the airflow, the longer the plume stays with the bubbles. For the case of crossflows, Socolofsky and Adams [2002] showed that prior to separation, the two-phase plume can be modelled as a mixed single-phase plume with B_0 as its initial buoyancy flux. After the separation, the now single phase plume behaves like a momentum jet. The bubbles that behave like a porous column follow a path directed by the sum of the bubble slip velocity (w_b) and the crossflow velocity (u_{cr}). The water entering the bubble plume above the separation height are deflected upward but they eventually leave the plume on the downstream side, see figure 2.6. An equilibrium between upstream capture and downstream loss is found. In figure 2.7 the separation height calculated following equation 2.29 is plot for crossflow velocities up to 0.7 m/s and airflows up to 250 Nl/min/m. Note the scale difference in the figures. In section 4.1 the effects of the separation height in the application of blocking plastics debris is investigated.

Larger bubbles rise slightly faster than smaller bubbles. With a crossflow present, smaller bubbles are therefore taken further by the current than larger ones. This phenomenon was first observed by Hugi in [1993] and is called fractionation, see figure 2.5 from Socolofsky and Adams [2002].

(a) 1 m increase per line

(b) 0.25 m increase per line
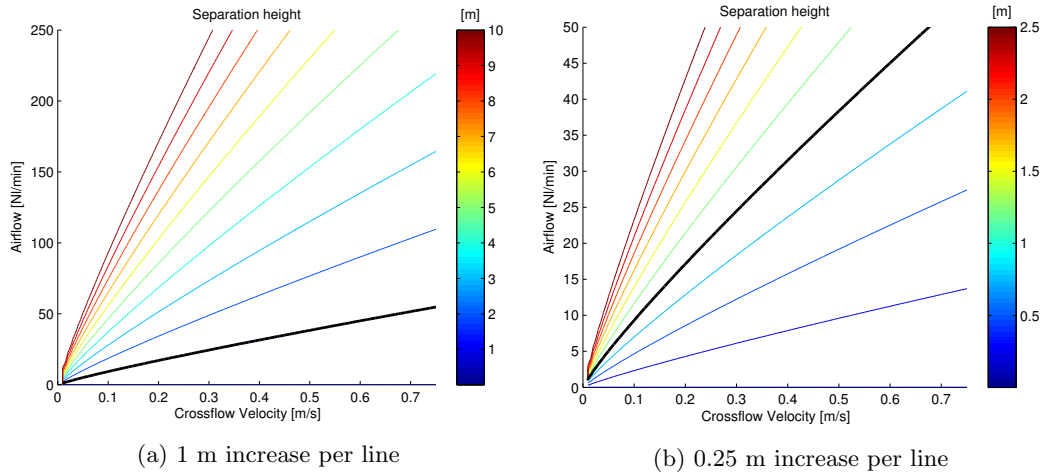
Figure 2.7: Separation height as a function of the crossflow velocity and the airflow. The thick black line represents a separation height of 1 m in both graphs.

2.7 Conclusion

The buoyancy of the bubbles drives them to surface while being taken by the crossflow. The rising bubbles entrain the ambient water, a plume of air and water is formed. The vertical velocity of this plume has a Gaussian profile, the highest velocities are reached in the centreline of the plume. The bubbles in the plume rise relative to the plume velocity with a constant bubble slip velocity. After the initial region the plume expands linearly moving upward from the tube, the shape can be described with variables z_0 and c which need to be determined from experiments. Based on the experiments a relation needs to be sought for these variables in order to predict the shape of the bubble curtain without performing experiments. The spreading and velocity of the plume vary depending on the airflow and the crossflow velocity.

For the case without crossflow, the vertical momentum is transferred into horizontal momentum when approaching the surface. The resulting horizontal flow induced by the bubbles reaches over the upper 25% of the water column. It can be felt up to four times the water depth away from the bubble screen in horizontal direction. The maximum velocity is reached at the surface close to the line of rising bubbles and the strength decreases linearly in depth and over distance away from the screen.

The research that has been performed on bubble curtains under a crossflow is mainly with the interest of aeration. Therefore they do not describe the induced horizontal flows that are the driving force of the bubble barrier in the function of blocking plastics.

The assumption is that the horizontal flow induced by the bubbles calculated for still water can be added to the logarithmic river profile to get the total horizontal surface flow field. Whether this assumption is valid follows from the comparison of the calculations and the experimental results.

The crossflow has a logarithmic profile because of friction. At the surface, the velocity is larger than the average velocity over depth. When the crossflow velocity is strong relative

to the airflow separation of the bubbles from the plume can occur.
Below the separation height, the plume consisting of air and water can be modelled as a
single-phase plume with the buoyancy of the bubbles as the initial driving force. This corre-
sponds to the description of the plume without a crossflow present. Thereby the assumption
that the rising plume can be described by the formula's from section 2.3 is substantiated.

Above the separation height, the water entering the plume is still deflected upward. However,
the water leaves the plume eventually at the downstream side and the horizontal flow induced
by the bubbles on the upstream side of the line of rising bubbles is much weaker than when
no separation occurs. The height at which this will occur can be calculated from the airflow
and the crossflow.

Chapter 3

Experiment Methodology

The calculations from the previous chapters miss values These values need to be found from experiments Also Experiments have been performed like this and this

To check the validity of the assumption that the horizontal flow induced by the bubbles is not affected by the crossflow, experiments have been performed in the Eastern Scheldt flume at Deltares. If the observations correspond with what is expected from the calculations, it will be possible to give a more substantiated design setup for other locations. The working of the bubble curtain depends mainly on the airflow, the crossflow and the angle of the curtain. These variables are varied in the experiments. This chapter discusses the setups at which has been tested, what has been measured and the method used to review the results.

3.1   Setup

The test facility has dimensions of 40x1x1.2 m with transparent walls. The maximum water level for the experiments is 1 m. There is a pump which can circulate water through the flume up to 600 l/s. With a water level of 1 m, the maximum crossflow velocity averaged over the depth and width is therefore 0.6 m/s. With the log profile calculated with formula 2.26 and the assumption of frictionless walls the maximum velocity at the surface is 0.71 m/s. The water level is regulated by adjusting the height of the flood wall at the end of the basin depending on the crossflow velocity. The depth-averaged flow velocities at which experiments have been performed are 0.05, 0.1, 0.2, 0.3, 0.4, 0.5 and 0.6 m/s with a water level of 1 m.

The tube setup has been adjusted in order to find the relation between the crossflow velocity, the angle of the tube relative to the flow direction and the required airflow to prevent the plastics from passing. Timewise only a couple of angles could be tested. The selected

Dimensions	40x1x1.2	m
Crossflow velocities	0.05, 0.1, 0.2, 0.3, 0.4, 0.5, 0.6	m/s
Airflow range	0-240	Nl/min
Angles	90, 63.4, 45, 26.6, 10	°

Table 3.1: Specifications of the flume and setups.

19
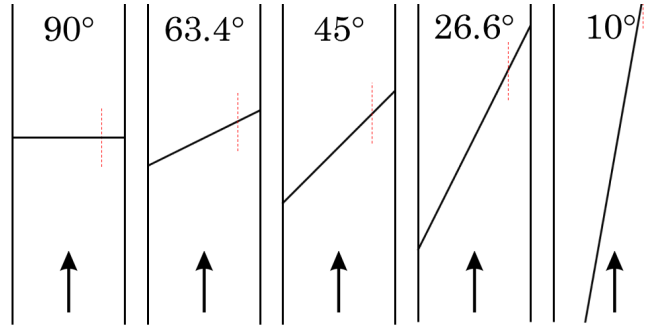
Figure 3.1: Top view of experimental tube setups.

angles are $90°, 63.4°, 45°, 26.6°$ and $10°$[1], see figure 3.1. At the $90°$ angle the tube lays perpendicular to the flow direction. This will certainly not result in an effective bubble barrier since the caught debris will not be led to the side of the river. Nevertheless, it gives insight into the working principle. Furthermore, it shows the effect of the walls of the flume, this is discussed in section 4.3.

At Deltares a compressed air network is available with a maximum capacity of about 240 l/min under atmospheric pressure conditions. An expression that is often used for this is the 'Normal litre'; 1 Nl has a volume of 1 litre under atmospheric pressure (1 bar or 10^5 Pa). The airflow can be adjusted with a valve (precision of 2 Nl/min). For smaller angles, a longer tube is needed to reach across the width of the flume. The maximum delivered airflow remains 240 Nl/min but this has to be distributed over more holes. When looking at the bubble-induced velocities, it is important to know the airflow per meter of tubing. Both the total airflow over the whole tube (Q_t) as the airflow per meter of tubing (Q_{atm} at the surface and Q_0 at the depth of the tube) is used in this research. The airflow over the whole tube can be measured with an airflow meter connected to the computer. This meter has an accuracy of 10^{-2} Nl/min.

For every combination of angle and crossflow velocity, different airflows have been tested to find a configuration that is able to redirect plastic debris to the side. Looking at the formulas for the horizontal flow velocity induced by the bubbles (2.6 and 2.23) it is expected that the higher the airflow the stronger the effect of the bubble curtain. However, when the airflow is too high it enhances turbulent motion of the water that can pull debris to deeper layers where it can pass through the bubble curtain more easily. Also in terms of energy consumption it is advisable not to overpower the system too much.

Pieces of different types and shapes of plastics have been selected to represent a variety of plastic debris present in nature. A list of the tested objects together with their density and the number of repetitions can be found in table 3.2.
Every tested configuration has been evaluated by means of the fraction of the plastic pieces of each type that was redirected into the corner by the bubble barrier. The 'corner' is defined to be within one-fifth of the width of the flume away from the wall at the downstream

---

[1]These seemingly odd angles have been chosen because when fixing the tube in the flume with tiles they are easy to get accurate. dx = 1 tile, dy = 2 tiles.

Table 3.2: Types of plastics used during flume experiments with their material and specific gravity

Object	Amount	Material	Specific gravity	Size $\pm20\%$ [cm]
Foam chips	10	expanded PS	0.003	2 x 1 x 1
Bottle caps	10	PE	0.91-0.97	⌀ 2 x 1
Balloons	4	Rubber	1.2	5 x 2 x 0.2
Partly filled bottles	2	PET, PS, H2O, air	variable	⌀ 5 x 20
Six-pack wraps	2			20 x 10 x 0.05
Thin bags	5	PE	0.91-0.97	35 x 20 x 0.01
Party cups	3	PS	1.04-1.07	⌀6 x 9
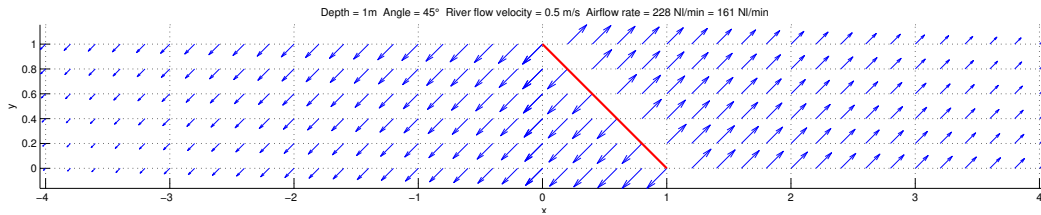
Figure 3.2: Top view of the horizontal flow field at the surface induced by the bubbles. The red line in the line of rising bubbles.

side of the bubble curtain see figure 3.1.

3.2 Resulting flow

In order to redirect the plastic debris floating in the upper layer to the side of the flume, the tube needs to lay at an angle. The horizontal flow field induced by the bubbles is always directed perpendicular to the line of the rising bubbles. The angle of the line of rising bubbles relative to the direction of the crossflow is called ϕ. For an angle ϕ of 45° a top view of the resulting surface flow field without a crossflow present can be seen in figure 3.2. This image is created in Matlab and it does not include the effect of the walls. In real life applications the width of the waterway will always be a lot more than 1 meter, therefore the calculations are performed assuming that the walls are not present.

To get the resulting flow profile, at every point the crossflow velocity should be added to the horizontal velocity induced by the bubbles, see figure 3.3. The direction of the resulting flow depends on the strength of the two velocities u_{cr}(y,z) and u_m(x,y,z) and the direction of u_m. The plastic particles are assumed to follow the path of the water it is surrounded by. Therefore the plastics should not pass through the bubble curtain if the resultant of u_{cr} and u_m remains on the upstream side of the line of rising bubbles. The angle of the resultant relative to the direction of the crossflow is called δ. In other words, angle δ should be larger than angle ϕ. The velocities u_{cr} and u_m are added for all the plotted points from figure 3.2, the result is shown in figure 3.4.
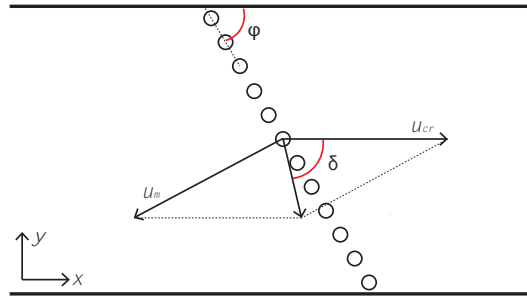
Figure 3.3: For every point the resultant of the crossflow velocity (u_{cr}) and the bubble-induced velocity (u_m) are added to get the flow profile. Top view.
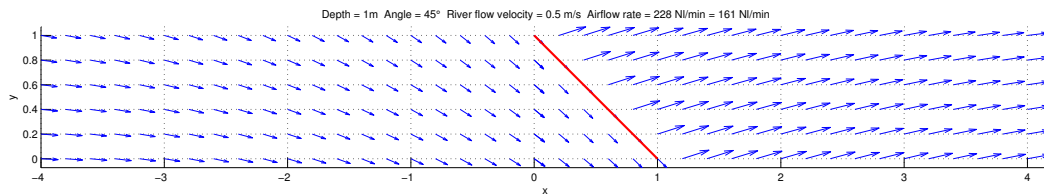
Figure 3.4: Top view of the horizontal flow field at the surface. The logarithmic river profile and the bubble-induced velocity profile are added.

In figure 3.5 a flow diagram of this system can be seen. In appendix ?? this scheme is shown in smaller sections allowing more detail. To calculate the direction of the resultant at height z the crossflow velocity and the bubble-induced velocity at that height need to be calculated as well as the angle of the line of rising bubbles.

To find the crossflow velocity at height z the equations for the logarithmic river profile from section 2.5 need to be filled in. However, in the flume it is not the slope but the pump that drives the flow. Therefore the formulas can not predict the magnitude of the crossflow. They can, however, be used to find the profile in depth when the depth-averaged velocity is known. To find the depth-averaged crossflow velocity the pump discharge can be divided by the cross-sectional area. Another way to find the depth-averaged crossflow velocity is to divide the x-displacement of the rising bubbles from the tube to the surface by the rising time. To find the rising time the vertical velocity of the plume needs to be calculated. How this is done is discussed in section 3.3 below. The way to calculate the bubble-induced horizontal velocity is discussed in section 3.4 below.

3.3 The rising plume

To measure the maximum vertical velocity in the centreline of the plume, bubbles rising up in the plume have been tracked in time. This can only be done for the 90° setups because it is required to look at the plume in the direction of the tube. Since the density of the plume is assumed to be equal to the density of water, the bubbles are rising with the speed of the
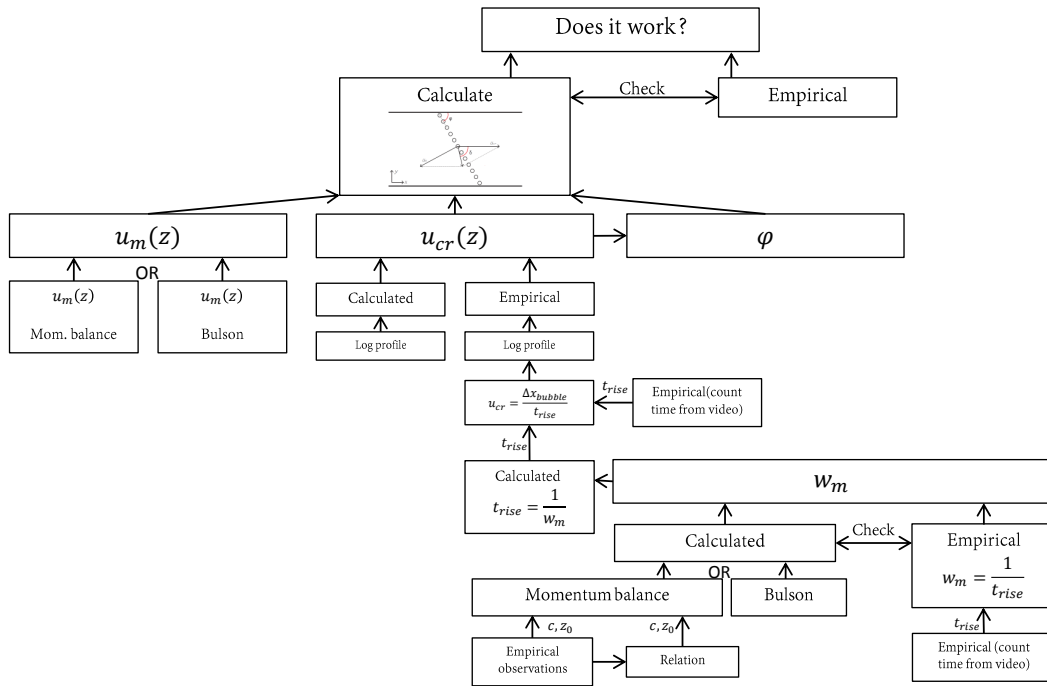
Figure 3.5: Scheme of research. To calculate the direction of the resultant at height (z), the crossflow velocity (u_{cr}) and the bubble-induced velocity (u_m) at that height and the angle of the line of rising bubbles (ϕ) need to be known. To check u_m the vertical velocity (w_m) needs to be known. Equations are checked with experimental observations.

plume plus the bubble slip velocity. The bubble slip velocity is assumed to be constant; w_b = 0.25 m/s. Whilst watching the video at 0.2 times the actual speed bubbles can be tracked from the moment they leave the tube until they reach the surface. Since many bubbles rise simultaneously it is hard to focus on one particular bubble, especially in the initial region. Therefore only the linear part of the rising plume[2] is counted. From the observed time and the depth of the linear part of the plume, the depth-averaged vertical velocity of the linear part can be derived.

The observed velocities are compared with the mean theoretical velocity over the linear part of the plume following the two available formulas. The first one is found by Bulson, he states that the vertical velocity is three-quarters of the maximum horizontal velocity calculated with equation 2.6. The second one is derived in section 2.3. Bulson's formula is not depth dependent. The derived equation calculates the vertical velocity of the centreline of the plume as a function of the height above the orifice (z). In order to use this formula the location of the analytical origin z_0 and the spreading ratio c need to be determined from the experiments first. To determine z_0 the linear boundaries of the plume as sketched in figure 2.3 are elongated in the downward direction. The depth of this cross section below the holes in the tube is the location of the analytical origin. The spreading ratio is determined following formula 2.16. The standard deviation of the Gaussian profile (σ) can be found by dividing the total width of the plume at height z by 6. By definition of the Gaussian profile, 6 σ includes 99.7% of the bubbles. After gathering these values the vertical velocity of the plume is calculated following both equations in section 4.2. The obtained velocities are compared to the observations.

3.4 Bubble-induced horizontal flow

In this section the method of comparing the calculated maximum horizontal surface velocities from both the momentum balance derived equation and Bulson's theory with the experiments will be discussed. Both equations are simplified for the case of the flume at Deltares.

The values corresponding to the flume can be filled in in equation 2.23. For the atmospheric pressure (p_{atm}), height of the bottom of the impingement zone (z_{imp}), the atmospheric pressure expressed as a head of water (H_0), the water depth (H), the density of water (ρ_w) and the bubble slip velocity (w_b). The formula can be written as:

$$u_m = \sqrt{\frac{-p_{atm}\ln(1 - \frac{z_{imp}}{H_0+H})}{0.25H\rho_w w_b}}\sqrt{Q_0} = 10.3\sqrt{Q_0} = 9.82\sqrt{Q_{atm}} \tag{3.1}$$

When expressing Bulson's formula in Q_0, for a tube laying in water of 1 m deep (on earth) it can be written as follows:

$$u_m = kg^{1/3}Q_0^{1/3} = 3.13Q_0^{1/3} = 3.03Q_{atm}^{1/3} \tag{3.2}$$

Now two formulas for the maximum horizontal flow velocity are formed. One is a square root function, the other a third root function. In figure 3.6 the formulas are plotted to $Q_t{}^3$.

---

[2]10 cm above the tube till the surface.

[3]Q_0 [m^3/s], Q_t [Nl/min]; $Q_0 = \frac{Q_t}{60*1000}\frac{H_0}{H_0+H}$
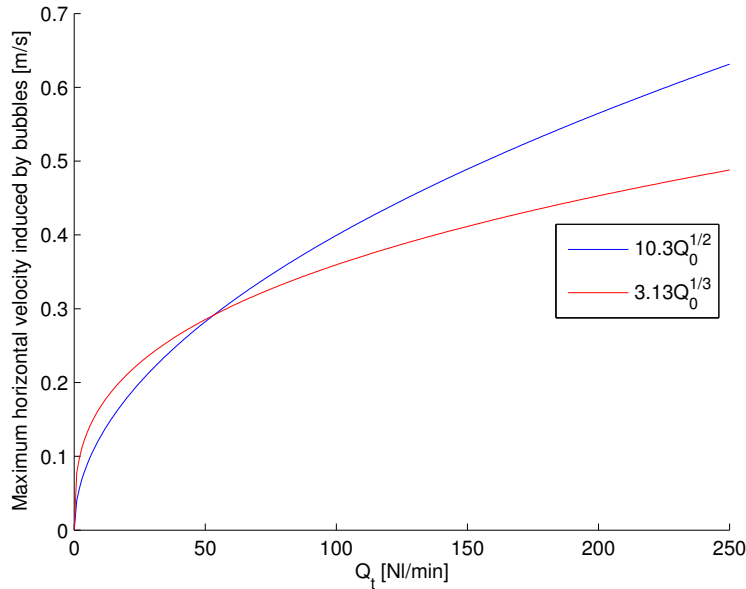
Figure 3.6: Maximum horizontal velocity calculated by the formula derived from the momentum equation 2.23(blue) and from Bulson's formula 2.6(red).

It can be seen that at an airflow of 53 Nl/min both formulas predict the same maximum horizontal airflow. With lower airflows, Bulson's formula gives larger velocities, with higher airflows the formula derived from the momentum balance predicts higher velocities. The maximum deviation of the two formulas is at the maximum airflow of 240 Nl/min. For the tube of 1 meter at a 90 ° angle the formula derived from the momentum balance and Bulson's formula predict a horizontal velocity of 0.62 m/s and 0.48 m/s respectively.

As stated in chapter 2 a linear decay in depth over the upper 25% of the depth of the water column is assumed. As well as a linear decay in horizontal distance from the line of rising bubbles over four times the depth in x-direction. Therefore, the horizontal flow at the surface close to the line of the rising bubbles is assumed to be maximum. And at 0.25 m depth, the horizontal flow velocity is zero. In figure 3.7 the horizontal flow induced by the rising bubbles is shown. Note that the impingement zone has a width (see figure 2.3) that is not present in this representation. Plastics should be stopped before entering the impingement zone, what happens inside the impingement zone is outside the scope of this research. Therefore, representing the flow without the impingement zone is justified. The effect of the bubble curtain on the horizontal flow in the lowest 75% of the water column is neglected. In figure 3.8 the logarithmic river profile is added to the bubble-induced velocity field. It can be seen that in the upper 25% of the water column the flow is slowed down upstream of the line of rising bubbles, and accelerated on the downstream side.

With the horizontal flow decreasing linearly over the upper 25 cm of the water column. This velocity decays both in depth as in horizontal distance from the line of the rising bubbles
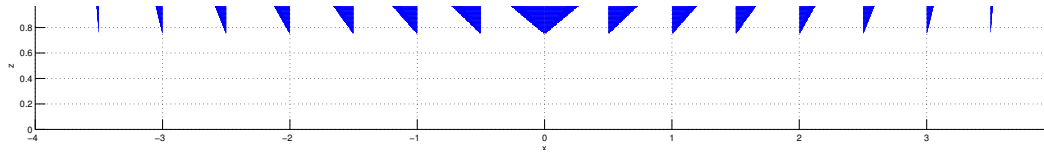
Figure 3.7: Side view of the horizontal flow field induced by the bubble curtain. The decay in depth and horizontal distance from the line of the rising bubbles.
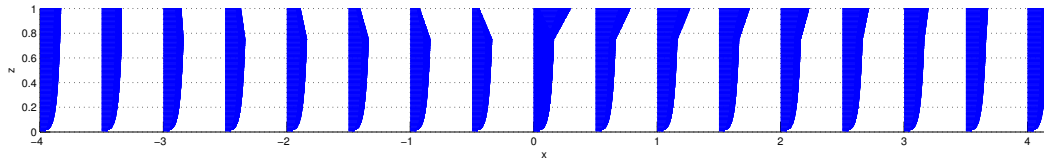
Figure 3.8: Side view of the summation of the logarithmic river profile and horizontal flow in the surface layer induced by the bubbles.

and is therefore very hard to measure in the laboratory without a proper velocimetry meter. It can, however, be seen whether the horizontal surface flow induced by the bubble curtain is sufficient to redirect the plastic particles following the theory of the resultant.

3.5 Conclusion

In this chapter, the method to predict the working of the bubble curtain in the function of redirecting plastic particles to the side has been explained. Experiments are performed in the flume at Deltares with dimensions of 40x1x1.2 m. All tests are performed at a water depth of 1 m and the maximum depth and width average crossflow velocity is 0.6 m/s. The angle of the tube relative to the flow direction as well as the crossflow velocity and the airflow are varied. Pieces of different types of plastics are put in the water to see whether they pass straight through the bubble curtain or are redirected into the corner.

For all the tested setups, the vertical velocity of a bubble in the centreline of the plume will be calculated following equations 2.7 and 2.20 and checked with the observations. Knowing the vertical velocity of the plume is important to check the depth-averaged crossflow velocity which in turn is needed to calculate the direction of the resultant of the horizontal flows. The maximum horizontal velocity induced by the bubbles is calculated following equations 3.1 and 3.2. They are compared to the experimental observations in section 4.3 to determine the most accurate method. If the resultant of u_{cr} and u_m at height z remains on the upstream side of the line of rising bubbles ($\delta > \phi$) it is assumed that a plastic particle at that height does the same and is therefore redirected into the corner.

Chapter 4

Flume results

In this chapter, the experiments will be used to check the validity of the calculations. First, some general observations on the bubble curtain in the flume will be presented. In order to calculate the vertical velocity with formula 2.20, the location of the analytical origin and the spreading ratio need to be determined from experiments. This will be done for all the setups tested at a 90° angle. An empirical relation will be formulated in order to calculate the vertical velocity without having to perform experiments. The crossflow velocity will be calculated from the vertical velocity. And form the crossflow velocity and the bubble-induced horizontal velocity the resultant of the flow can be calculated. The theoretical predictions will be compared with the experimental results.

4.1 General flume observations

Before looking at the ability of the bubble barrier to block plastics, first, the behaviour of the plastics in the water column and the general behaviour of the bubble curtain will be discussed. The most convenient setup for observations is when the tube lays at a 90° angle relative to the flow direction. This setup gives a clear side view as can be seen in figure 4.1. All setups tested at a 90° angle are listed in table 4.1.

General behaviour plastic objects

The types of plastics that have been tested are listed in table 1.1 with their properties and size. In this section, the behaviour of each type of plastics in the flume with a crossflow is elaborated. As expected the foam chips float on top of the water, they follow the path of the most upper layer of the water column and they would be very much affected by the wind if present.
The bottle caps float just underneath the surface, with the opening either on the top or bottom. They follow the upper 1.2 cm of the water column. The wind has no direct effect on them. However, the most upper layer of the water column is affected by the wind.
Even though the specific gravity of rubber is 1.2, the balloons are floating in the upper layer of the water column touching the surface. This possibly results from air being caught inside the balloon even though they were cut open. Sometimes they lay horizontally under the surface, other times they hang vertically and reach deeper.
One of the bottles was half full, the other one was filled for three quarters. The water depths

Table 4.1: Setups at a 90° angle

#	Angle [°]	u_{cr} [m/s]	Q_t [Nl/min]
1	90	0.05	1.5
2	90	0.05	3.4
3	90	0.1	12.7
4	90	0.1	16.2
5	90	0.1	23
6	90	0	30
7	90	0.2	102
8	90	0.2	120
9	90	0.2	228
10	90	0.3	228
11	90	0.4	228
12	90	0.5	228
13	90	0.6	228

they reach as well as the sensitivity for wind depend strongly on the amount of water inside and their orientation.

The six-pack wraps are fully submerged but keep touching the surface. If they catch air from the bubble curtain they can partly get above the surface.

As well as the six-pack wraps the thin bags are fully submerged when no air is caught inside. However, they do not necessarily touch the surface. When dividing the water column into four parts in the vertical, about 0, 10, 20 and 70% flows in the firsts, second third and fourth quarter from the bottom respectively. When reaching the bubble curtain the bags tend to catch less air than the sick pack wraps, especially when deeper in the water column.

The cups are rolling along the bottom of the flume. A few times a cup arrived at the bubble curtain upside down, caught air and floated afterwards. Only in this situation, the cups can sometimes be blocked by the bubble barrier, else they are not affected. This research focuses on floating plastic debris and therefore the cups are not taken into account in the results.

Undulating motion of the plume

Looking at the bubble curtain at a 90° angle without a crossflow present it can be seen that the bubble curtain is undulating. In time the bubbles spread out to the right or left when looking at the plume from the side. This effect is not equal over the full width of the flume. When looking from the top the line of the rising bubbles is curved. A side view at three time instances can be seen in figure 4.1. The full time-lapse can be found in appendix **??**. This undulating motion is enhanced by turbulence in the rising plume. In this research, turbulence is not taken into account. Simiano et al. [2009] have looked into oscillation of a point source bubble plume. They state that the results are not yet well understood and sometimes contradictory, in particular concerning turbulence.

In his experiments Kobus [1968] averaged all his results over a five minute time interval.

(a) t = 10 s   (b) t = 25 s   (c) t = 40 s
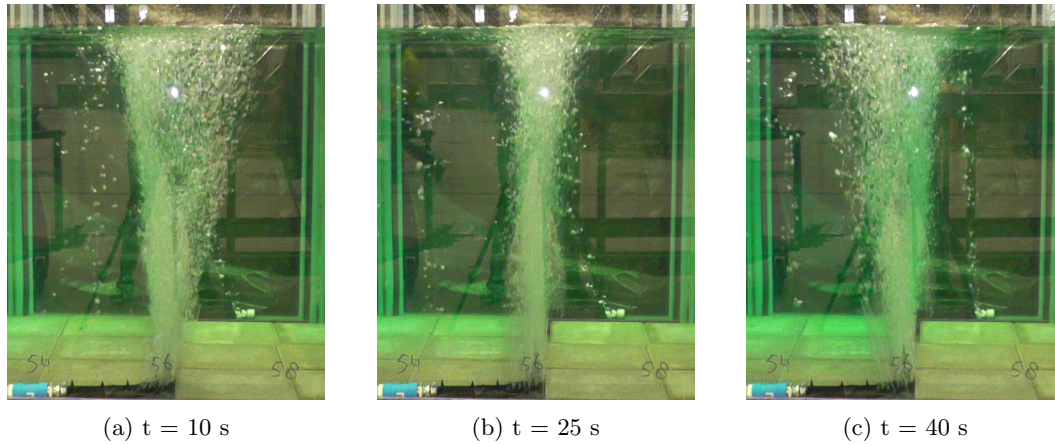
Figure 4.1: Side view of the bubble plume at a 90° angle and airflow of 30 Nl/min/m with no lateral flow present. At three time instances.

Because of the undulating motion of the plume, he found larger widths and smaller centreline velocities than actually occurred. In order to obtain accurate values for the spreading ratio and the location of the analytical origin, there should not be averaged over a too large time interval. It is, however, important for the reliability of the research not to draw conclusions from a single time instance. Therefore a characteristic time scale is defined as the rising time of the bubble. The rising time of a bubble in the plume can be found by dividing the depth by the rising velocity of a bubble in the plume. The results will be averaged over 10 times this characteristic time.

$$t_c = \frac{Depth}{Rising\ velocity} \tag{4.1}$$

The rising velocity can be determined following formula 2.20 to obtain the maximum velocity of the water in the centreline of the plume. To this maximum velocity of the water in the plume, the bubble slip velocity of 0.25 m/s should be added to obtain the maximum vertical velocity of a bubble in the plume. However, the spreading ratio (c) and the location of the analytical origin (z_0) that need to be filled in can only be determined when the averaged results are available. To circumvent this the rising time is determined from the observations from the flume.

Observed rising time for the 90° angle and airflow of 30 Nl/min/m with no lateral flow present is 1.4 s. Therefore the time over which should be averaged is 14 s. Averaging over a 14-second interval could in this case still result in somewhat wider plumes and faster rising bubbles. Nevertheless, in order to obtain reliable results this should be seen as a necessary limitation.

In order to say something about the average over the defined time interval, Matlab's image averaging has been used. In figure 4.2 the averaged picture can be seen for the same setup as before between t=20 and t=34 s as in appendix ??.

Figure 4.2: Averaged image of 90°, 0 m/s, 30 Nl/min

Lateral spreading of the bubbles

In figure 4.2 it can be seen that the centreline of the plume has the highest density of bubbles, suggesting a Gaussian profile of the bubbles in the horizontal plane. Since accurate measurements of the velocity are lacking it is very hard to say something about the shape of the velocity profile. However, since the upward velocity is induced by the density difference which is in turn induced by the bubble fraction it can be stated that the assumption of a Gaussian profile for the velocity as well as the density difference is accurate.

Separation height

In appendix ?? the influence of the separation height on the behaviour of the bubble curtain is shown. Different setups are shown with their separation height. The smaller the separation height the closer the plastic particle approach the middle of the line of rising bubbles. However, plastics can still be led to the corner even when the separation height is smaller than the depth. The system seems to be more reliable when the separation height is larger than the depth. This is, therefore, a factor to take into account when designing a bubble barrier.

4.2   Vertical velocity of the rising plume

In order to calculate the theoretical vertical velocity at the centre of the plume over the depth following formula 2.20, values for the spreading ratio (c) and the location of the analytical origin below the tube (z_0) need to be known. These values have to be determined
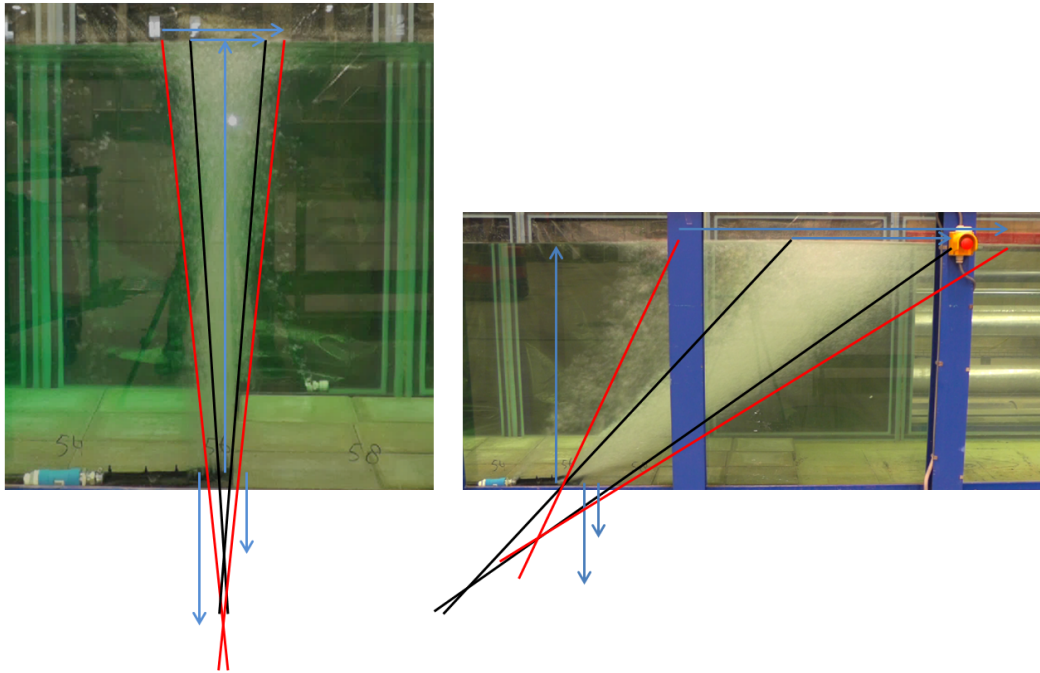
Figure 4.3: Side view from the flume with a bubble curtain at 90°, 0 m/s, 30 Nl/min on the left and 90°, 0.3 m/s, 228 Nl/min on the right

from the experiments by looking at the linear spread of the plume. The amount of air bubbles contained in the plume is hard to count and therefore it is hard to define the edge of the plume. The edges should be defined such that 99.7% of the bubbles is within these boundaries[1]. Therefore, a narrow (black) and a wide (red) version have been determined. In figure 4.3 a time averaged[2] side view of the plume is shown with the boundaries sketched for both the narrow and the wide version. For both versions, the width of the plume at the surface (horizontal arrows at the top) and the location of the analytical origin (vertical arrows at the bottom) have been sketched. The spreading ratio can be determined following formula 2.16 taking the width of the plume at the surface as six times the standard deviation (σ). For this situation at 90°, 0 m/s, 30 Nl/min the narrow option leads to $z_0 = 0.18$ m and $c = 0.023$ and the wide option to $z_0 = 0.33$ m and c = 0.035. For the situation at 90°, 0.3 m/s, 228 Nl/min the narrow option leads to $z_0 = 0.42$ m and c = 0.079 and the wide option to $z_0 = 0.23$ m and c = 0.188.

The values for z_0 and c have been determined for all configurations at a 90° angle. The results of this can be seen in table 4.2. A very limited amount of setups has been performed. In most cases, both the crossflow velocity and the airflow have been changed. This makes it hard to compare different cases and make clear conclusions. Setups 9-13 from table 4.2 do, however, have the same airflow. Together with their linearly increasing crossflow velocity, this makes them suitable for comparison. The location of the analytical origin, as well

---

[1]By definition of the Gaussian profile this percentage is within the $\pm 3\sigma boundaries$.
[2]See section 4.1 for explanation.

Table 4.2: Setups at a 90° angle. N(arrow), W(ide)

#	Angle [°]	u_{cr} [m/s]	Q_t [Nl/min]	z_0 [m] N	W	c N	W
1	90	0.05	1.5	0.39	0.19	0.012	0.024
2	90	0.05	3.4	0.34	0.34	0.015	0.026
3	90	0.1	12.7	0.22	0.20	0.023	0.044
4	90	0.1	16.2	0.31	0.11	0.019	0.050
5	90	0.1	23	0.22	0.27	0.025	0.045
6	90	0	30	0.27	0.33	0.023	0.035
7	90	0.2	102	0.35	0.07	0.050	0.132
8	90	0.2	120	0.29	0.10	0.044	0.130
9	90	0.2	228	0.26	0.15	0.064	0.140
10	90	0.3	228	0.42	0.23	0.079	0.188
11	90	0.4	228	0.29	0.10	0.115	0.268
12	90	0.5	228	0.33	0.11	0.113	0.297
13	90	0.6	228	0.49	0.14	0.138	0.374

as the spreading ratio of these cases, are plotted in figure 4.4. In figure 4.4b, linear lines are plotted through the points from the narrow and the wide option. The area between these lines (grey) gives an estimate of the region in which the spreading ratio should lay at different crossflow velocities for an airflow of 228 Nl/min/m. In figure 4.4a the same area is plotted for the location of the analytical origin, however in this case, the relation does not seem to be reliable.

Looking at values of c for setups with constant crossflow velocities in table 4.2, like setups 3 to 5. The spreading ratio does not seem to increase with airflow. When comparing setup 3 and 6 it can be seen that even with double the airflow, the spreading ratio did not increase at all. The spreading ratio seems to be independent of the airflow. For each crossflow velocity the values of c are averaged, for both the narrow and the wide option. The resulting values are plotted in figure 4.5 with a line fitted by Matlab through the mean values. Setup 6 has a crossflow velocity of 0 m/s and since the relation depends on the crossflow velocity this setup is excluded. The line happens to cross the origin and can be described by the following formula:

$$c = 0.433 \, u_{cr} \tag{4.2}$$

With this formula, the spreading ratio can be determined. It only depends on the crossflow velocity. It is assumed that the airflow is not influencing the spreading ratio.

Looking at table 4.2, the location of the analytical origin does not seem to follow a trend. All values of z_0 are represented in boxplots in figure 4.6, one for the narrow options and one for the wide options. The narrow options have on average higher values for the location of the analytical origin. With mean values of 0.31 m for the narrow option and 0.15 m for the wide option. The influence of changing this value will be discussed later in this section.

When the vertical velocity in the centreline of the plume is calculated with formula 2.20 it depends on the height above the tube (z). The vertical velocity profile of setup 6 with the values of z_0 and c from table 4.2 is plot in figure 4.7. The vertical velocity profile over the vertical is plotted for the narrow (black) and the wide (red) option. The dashed lines are
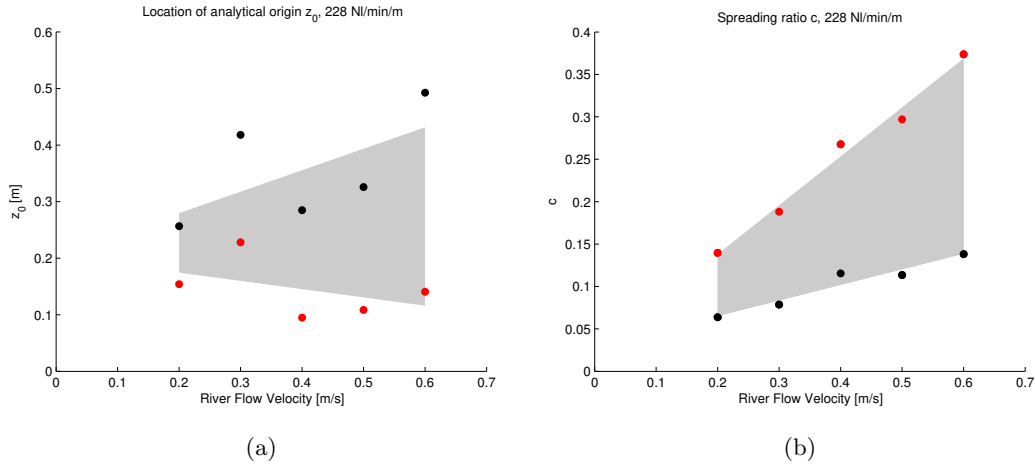
Figure 4.4: Spreading ratio with changing crossflow velocities at an airflow of 228 Nl/min/m. Black (Narrow) and Red (Wide)
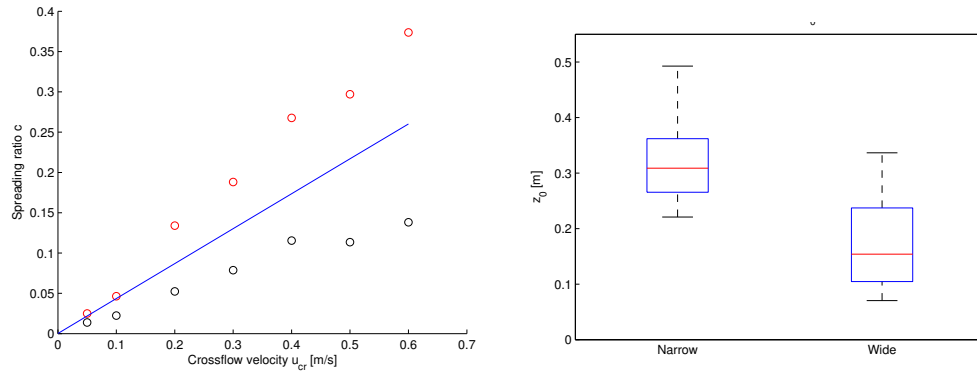
Figure 4.5: Black and red dots are averaged values of c for the narrow and wide option respectively per crossflow velocity. Blue line is fitted through the mean of the two points per velocity.

Figure 4.6: Boxplot of the values of z_0 for the narrow (left) and wide (right) version at all 90° setups.
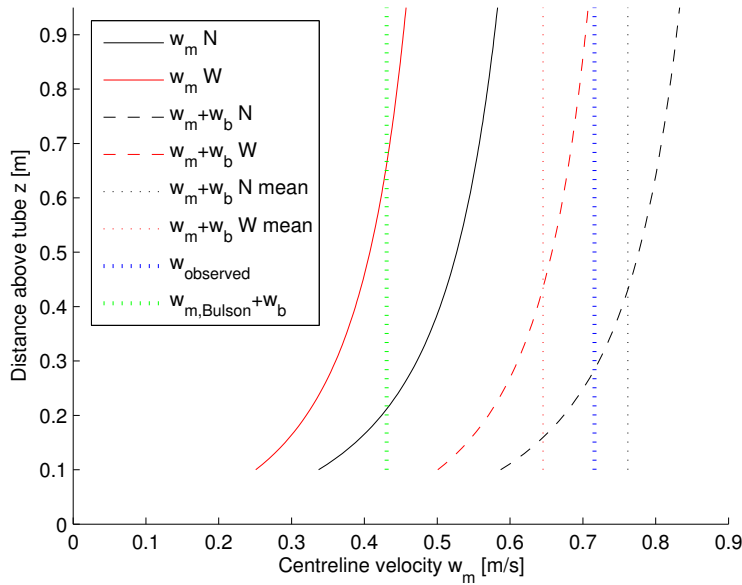
Figure 4.7: Centreline velocities compared for the case $90°$, 0 m/s, 30 Nl/min.

these velocity profiles with the bubble slip velocity added, they represent the total velocity of a bubble in the plume. The dotted black and red lines are the depth average[3] of the velocity profiles. The green dotted line is the centreline velocity calculated with Bulson's formula with the bubble slip velocity added. The blue dotted line represents the average observed velocity. It can be seen that this value is between the two boundaries, narrow and wide. Bulson's prediction is way smaller than the observed value. The value calculated on the formerly explained way seems to match the observations better. In table 4.3 the depth-averaged vertical centreline velocities are shown for all setups calculated with both formulas. When comparing the calculated values to the observations, it can be seen that equation 2.20 gives better results for all setups than Bulson's formula. Figure 4.8 shows the vertical velocities from table 4.3 to the airflow. The shape of the points represents the crossflow velocity. The blue points are the observed values. The green points are calculated following Bulson's formula. The magenta points represent the average of calculated values for the narrow and the wide option following equation 2.20.

It can be seen that the vertical velocity increases with an increasing airflow as would be expected looking at formula 2.20. However, when the airflow remains constant but the crossflow velocity increases (setup 9 to 13) the vertical velocity gets smaller. This can be explained since, with a higher crossflow present, the bubbles spread more in the lateral direction. Therefore the density of the bubbles decreases and the maximum vertical velocity decreases too. The vertical momentum that is transferred, however, remains constant.

---

[3]Over the linear part of the plume, from 10 cm above the tube till the surface.

Table 4.3: Vertical velocity of a bubble in the centreline of the plume. Calculated with equation 2.7 and equation 2.20 and observed from the experiments.

#	Q_t [Nl/min]	u_{cr} [m/s]	$w_{m,Bulson} + w_b$ [m/s] green	$w_{m,Mom} + w_b$ [m/s] W red		mean magenta	N black	$w_{m,Observed}$ [m/s] blue
1	1.5	0.05	0.32	0.37	0.38	0.39	0.39
2	3.4	0.05	0.34	0.40	0.43	0.45	0.46
3	12.7	0.1	0.39	0.50	0.54	0.59	0.54
4	16.2	0.1	0.40	0.54	0.59	0.65	0.56
5	23	0.1	0.42	0.57	0.63	0.69	0.68
6	30	0	0.43	0.65	0.70	0.76	0.72
7	102	0.2	0.52	0.71	0.78	0.85	0.73
8	120	0.2	0.54	0.74	0.85	0.97	0.74
9	228	0.2	0.60	0.87	0.98	1.10	0.94
10	228	0.3	0.60	0.75	0.85	0.94	0.82
11	228	0.4	0.60	0.72	0.79	0.87	0.79
12	228	0.5	0.60	0.69	0.77	0.86	0.74
13	228	0.6	0.60	0.63	0.69	0.75	0.69
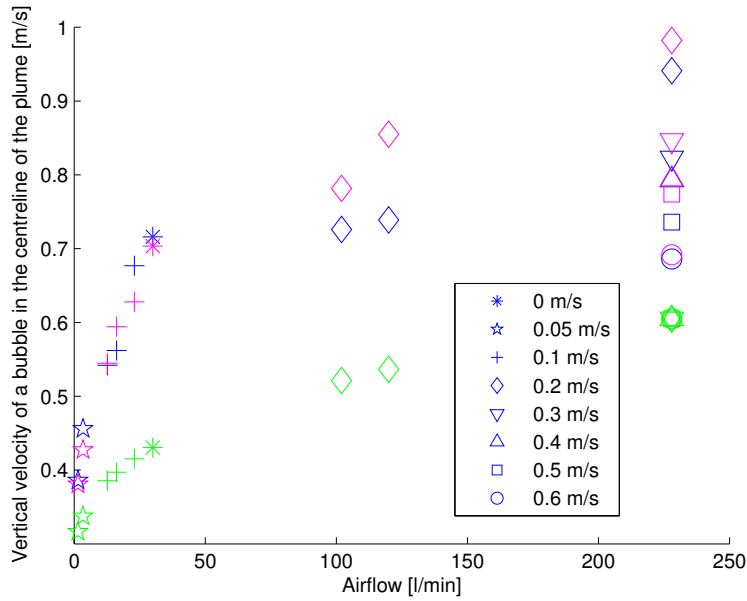
Figure 4.8: Observed vertical velocities compared with calculated values. For the colour codes see table 4.3.

Table 4.4: Vertical velocities calculated with equation 2.20 and different values for c and z_0. With the error of w_m with the values of the first w_m column relative to w_m of the certain column.

#	w_m [m/s]	w_m [m/s]	error [%]	w_m [m/s]	error [%]	w_m [m/s]	error [%]	w_m [m/s]	error [%]
c	per case	formula		formula		formula		formula	
z_0	per case	per case		0.23 m		0.15 m		0.31 m	
	magenta	yellow	square	red	circle	cyaan	circle	black	circle
1	0.38	0.37	4.2	0.38	0.8	0.37	2.9	0.36	4.7
2	0.43	0.42	2.3	0.44	3.4	0.43	0.8	0.42	1.5
3	0.54	0.50	9.0	0.51	6.2	0.50	9.6	0.48	12.6
4	0.59	0.54	10.9	0.55	8.7	0.53	12.3	0.51	15.5
5	0.63	0.58	8.5	0.60	4.0	0.58	7.8	0.56	11.2
6	0.70								
7	0.78	0.76	2.7	0.78	0.7	0.74	4.9	0.72	8.7
8	0.86	0.81	6.2	0.82	4.1	0.79	8.7	0.76	12.7
9	0.98	1.00	2.2	1.04	5.3	0.99	0.8	0.95	3.3
10	0.85	0.82	3.2	0.89	5.2	0.85	0.9	0.82	3.0
11	0.79	0.79	0.0	0.81	1.6	0.77	2.7	0.75	6.5
12	0.77	0.73	6.4	0.75	3.5	0.72	7.8	0.69	11.6
13	0.69	0.66	4.6	0.70	1.8	0.68	2.1	0.65	5.6
avg			5.0		3.8		5.1		8.1

Influence of c and z_0

To check the validity of the obtained relation for c, the vertical velocities are calculated with c per case and from the relation. The resulting vertical velocities can be seen in table 4.4. The first w_m column contains the mean value of the narrow and the wide option calculated with c and z_0 determined empirically per case. It can be seen that the average error of the vertical velocities calculated with the relation for c compared to the velocities calculated with c per case is 5%. Figure 4.9 shows this influence of changing the spreading ratio per setup. The grey bars represent the vertical velocity range from the narrow to the wide option, with the empirically found values for c and z_0. Also the influence of taking $z_0 = 0.15$, 0.31 or the mean of 0.23 meter is checked. For the comparison c is taken from the relation, the resulting vertical centreline velocities are listed in table 4.4 and shown in figure 4.10. It can be seen that the average error of all the cases is lowest when for z_0 the value of the wide option 0.15 m is taken. For this case, the all calculated vertical velocities are within 10% of the value calculated with the empirically determined c and z_0.
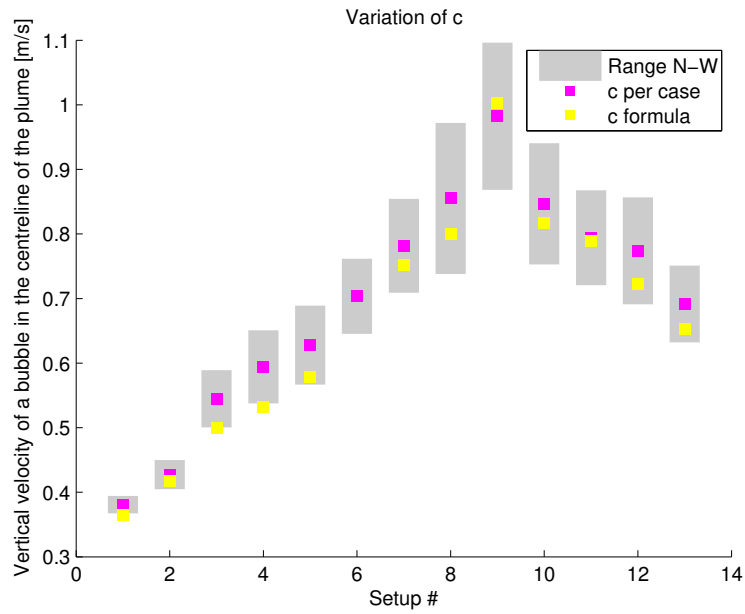
Figure 4.9: Vertical velocities calculated following formula 2.20 with a constant bubble slip velocity of 0.25 m/s added. Influence of varying c.
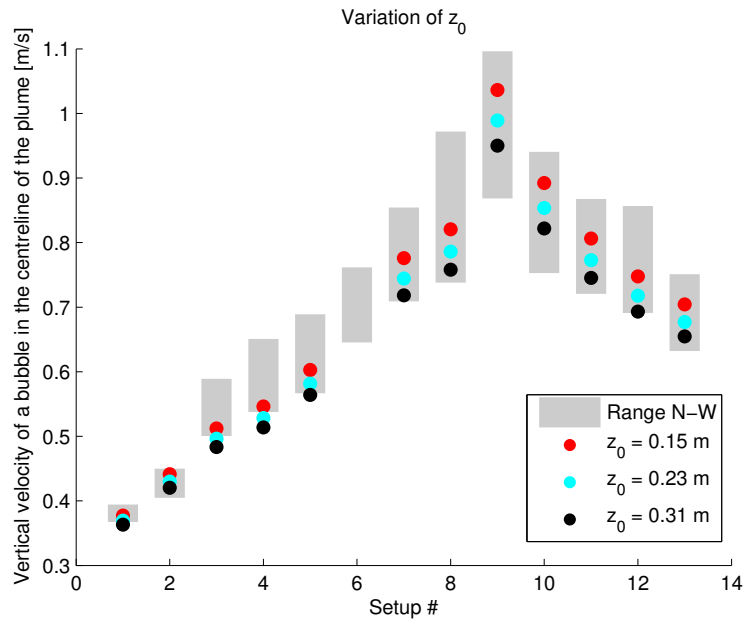
Figure 4.10: Vertical velocities calculated following formula 2.20 with a constant bubble slip velocity of 0.25 m/s added. Influence of varying z_0.

Table 4.5: Average crossflow velocity calculated with the travelled distance in x-direction.

#	Q_t [Nl/min]	$u_{cr,avg}$ [m/s]	w_m [m/s]	w_{mean} [m/s]	t_{rise} [s]	dx_{min} [m]	dx_{max} [m]	$u_{cr,min}$ [m/s]	$u_{cr,max}$ [m/s]	h_s [m]
1	1.5	0.05	0.38	0.16	6.02	0.1	0.25	0.02	0.04	0.30
2	3.4	0.05	0.44	0.18	5.14					0.67
3	12.7	0.1	0.51	0.21	4.43					1.36
4	16.2	0.1	0.55	0.23	4.16					1.74
5	23	0.1	0.60	0.25	3.77	0.3	0.45	0.08	0.12	2.47
6	30	0	Inf							
7	102	0.2	0.78	0.32	2.93	0.6	1	0.20	0.34	5.96
8	120	0.2	0.82	0.34	2.77	0.55	1	0.20	0.36	7.01
9	228	0.2	1.04	0.43	2.19	0.5	1	0.23	0.46	13.31
10	228	0.3	0.89	0.37	2.55	0.7	1.3	0.27	0.51	9.32
11	228	0.4	0.81	0.34	2.82	1.2	1.8	0.43	0.64	7.23
12	228	0.5	0.75	0.31	3.04	1.4	2.2	0.46	0.72	5.94
13	228	0.6	0.70	0.29	3.23	1.6	2.9	0.50	0.90	5.06

4.3 Bubble-induced horizontal flow

In this section, the horizontal flow near the surface induced by the rising bubbles will be investigated. Two equations are available that predict the maximum horizontal velocity induced by the flow, the first is derived from the momentum balance in section 2.4 and the second is empirically found by Bulson, see section 2.2. Together with the crossflow velocity and the angle of the tube a prediction is made on whether the bubble curtain will redirect plastics to the side or not. This prediction is compared to the experimental results.

Crossflow velocity

No tests have been performed without pumping air through the tube. Therefore the only way to calculate the depth-averaged crossflow velocity is by looking at the angle of the deflected plume relative to the vertical, see figure 2.7.

The values for the crossflow in table 4.5 are calculated with the displacement in x-direction of a bubble and the mean rising velocity of the plume[4]. Except for setup 1, all crossflow velocities seem to be within the range of the width of the plume.

Bubble-induced horizontal flow at a 90° angle

In chapter 2 the physics of the horizontal flow have been discussed and in chapter 3 the variables for the flume at Deltares have been filled in in the equation derived from the momentum balance (3.1) and Bulson's relation (2.6). The resulting equations are:

$$u_m = 10.3\sqrt{Q_0} \tag{4.3}$$

$$u_m = 3.13Q_0^{1/3} \tag{4.4}$$

Table 4.6: Maximum horizontal velocity calculated with formula 4.3.

#	u_{cr} [m/s]	Q_t [Nl/min]	u_{mMom} [m/s]	$u_{mBulson}$ [m/s]
1	0.05	1.5	0.05	0.09
2	0.50	3.4	0.07	0.12
3	0.1	12.7	0.14	0.18
4	0.1	16.2	0.16	0.20
5	0.1	23	0.19	0.22
6	0	30	0.22	0.24
7	0.2	102	0.40	0.36
8	0.2	120	0.44	0.38
9	0.2	228	0.61	0.47
10	0.3	228	0.61	0.47
11	0.4	228	0.61	0.47
12	0.5	228	0.61	0.47
13	0.6	228	0.61	0.47

The resulting maximum horizontal velocity for all the 90° setups can be seen in table 4.6. To check the validity of these calculations can be checked as follows. The calculated maximum horizontal velocity of setup 3 with an airflow of 12.7 Nl/min equals 0.14 (Mom) or 0.18 (Bulson) m/s depending on the chosen equation. Since the crossflow velocity of this setup is 0.1 m/s it is expected that the plastic particles that float in the upper 7.5 or 11 cm[5] of the water column would be stopped. Looking at figure 4.11 this seems to be correct. The calculated maximum horizontal velocity at an airflow of 228 Nl/min equals 0.61 or 0.47 m/s. Therefore in an ideal case, even with a crossflow velocity of 0.4 m/s, the foam chips and bottle caps would not pass the line of rising bubbles since they are only in contact with the most upper layer where the horizontal velocity is largest. However, the situation is far from ideal. The higher crossflow velocity and airflow induce a wall effect. The large bubbles rising at the walls (see figure 4.13) form a funnel that leads most of the debris through in the middle of the flume. Even at a crossflow velocity of 0.2 m/s, this effect can be seen. The foam chips are blocked, but the bottle caps are not (see figure 4.12).

The stronger the crossflow the clearer the funnel effect is, figure 4.14 shows the top view of setup 12 with an airflow of 228 Nl/min and a crossflow velocity of 0.5 m/s. At other angles of the tube, this effect is different since the x-location of where the tube hits the wall is different for both ends.

The horizontal flow field with the tube at an angle

When the tube lays under an angle the direction of the resultant of the crossflow velocity and the bubble-induced velocity can be determined at every height. This is explained in section 3.4. This direction is expressed as the angle relative to the direction of the crossflow (δ). Therefore, the angle δ increases with increasing airflow and decreases with increasing crossflow velocity. The direction of the resultant is calculated with both formulas with the tube at a 45° angle at a depth of 1 cm. This includes the foam chips and the bottle caps.

---

[4]Taking the integral over the Gaussian profile; $w_{mean} = 0.4178 * w_m$

[5]$0.25(1 - 0.1/0.143) = 0.075$

(a) t = 0 s   (b) t = 7 s   (c) t = 14 s
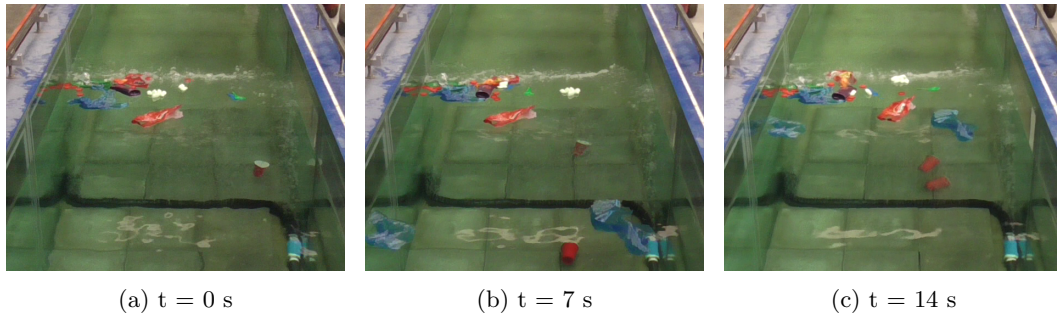
Figure 4.11: Top view of setup 3 (0.1 m/s, 12.7 Nl/min) from table 4.6. At three time instances.

(a) t = 0 s   (b) t = 10 s   (c) t = 20 s
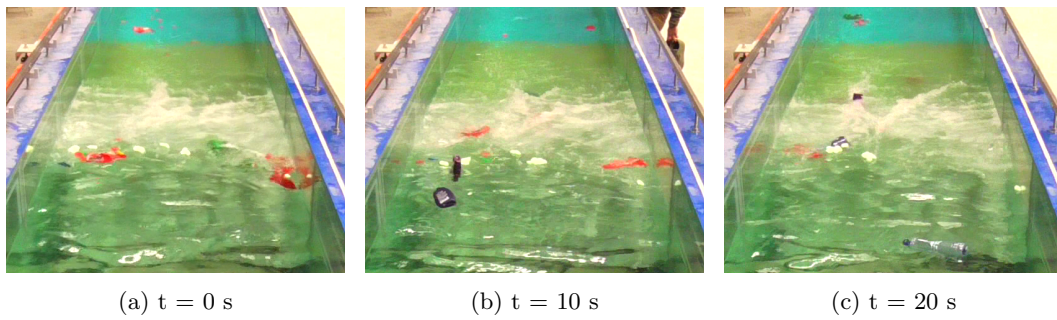
Figure 4.12: Top view of setup 9 (0.2 m/s, 228 Nl/min) from table 4.6. At three time instances.

Figure 4.13: Side view of setup 9 (0.2 m/s, 228 Nl/min).

Figure 4.14: Top view of setup 12 (0.5 m/s, 228 Nl/min).

The total airflow (Q_t) ranges from 0 to 250 Nl/min (under this angle 0 to 171 Nl/min/m). All the crossflow velocities at which is tested in the flume are represented by a line in figure 4.15. The horizontal line represents ϕ the angle of the tube relative to the direction of the crossflow. If one of the lines crosses this horizontal line it means that the resultant is going from downstream to upstream of the line of rising bubbles ($\delta=\phi$). The corresponding airflow is required to block the plastics.

These calculations are compared with the performed experiments. In figure 4.15 the points represent a certain tested setup. The line at which a point lays represents the depth-averaged crossflow of the experiment. On the x-axis, the airflow over the whole tube of the certain setup can be found. For example, one setup has been performed with a crossflow of 0.3 m/s (light blue line) and an airflow of 49 Nl/min. At this point, a pentagram can be found. The shape of the points represents the effectiveness of the certain setup looking at the foam chips and the bottle caps. A circle means that all foam chips and bottle caps were redirected into the corner. A square means that more than 90% of the foam chips and bottle caps were redirected. A pentagram means that less than 90% was redirected into the corner. The numbers next to the points represent the separation height calculated following formula 2.29. It is important to know the separation height since it influences the effectiveness of the bubble barrier, as has been discussed in section 4.1. In appendix ?? the resulting plots for the other angles of the tube can be found.

When taking a close look at the results of $\phi = 45°$ the following can be seen. In the upper plot, at low crossflow velocities the bubble barrier is already working when the calculations state it should not (circles below the line). While at high crossflow velocities, airflows that are predicted to be effective are not (pentagrams above the line). The prediction of the lower plot is also not sufficient since there are pentagrams above the horizontal line. However, the error seems to be more constant. In this case is a safety factor would be added or the resultant would be calculated at a deeper point (3.5 cm), the prediction would correspond.

The horizontal velocity induced by the bubbles decreases linearly in depth over the upper 25% of the water column. Whereas the crossflow velocity decays logarithmically over the whole water column. Therefore when calculating the resultant of these two velocities at higher depths, the angle of the resultant gets rapidly smaller. The predicted required airflow increases. In figure 4.16 the result of looking at higher depths is shown for the case of $\phi = 45°$ and $u_m = 0.2$ m/s calculated with Bulson's formula (the red line of figure 4.15b).

For the other angles:
$\phi = 63.4°$: Both formulas give pretty bad results. Bulson's solution seems to be more constant in the error. If the resultant is calculated at a depth of 8 cm, the line seems to predict the required airflow well
$\phi = 26.6°$: On the first sight the upper figure seems to give better results, but both figures predict airflows that are not sufficient. When looking at deeper resultants, Bulson's formula gives better results. At a depth of 5 cm, the line predicts the required airflow well.
$\phi = 10°$: Bulson's formula is not correct for the low crossflow velocities. This is not scalable because the higher crossflow velocities would need infinite air, but they do not. The upper figure gives more constant results, if the resultant is calculated at a depth of 3.5 cm it gives accurate predictions. The separation height of all setups is very low, this may cause the changing behaviour.
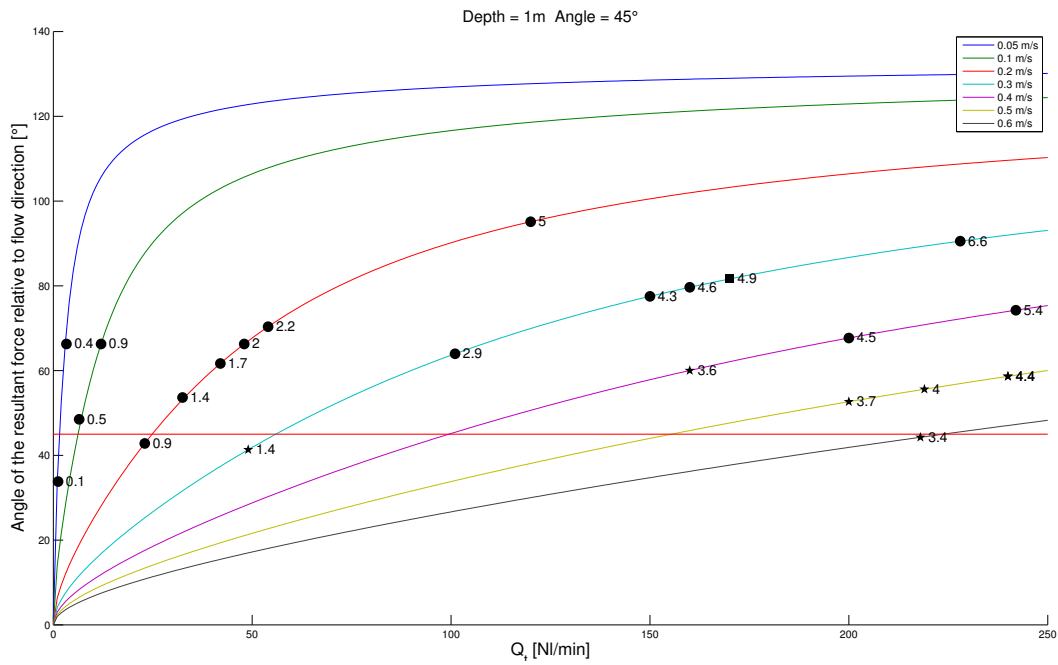
(a) 45° angle. Momentum balance
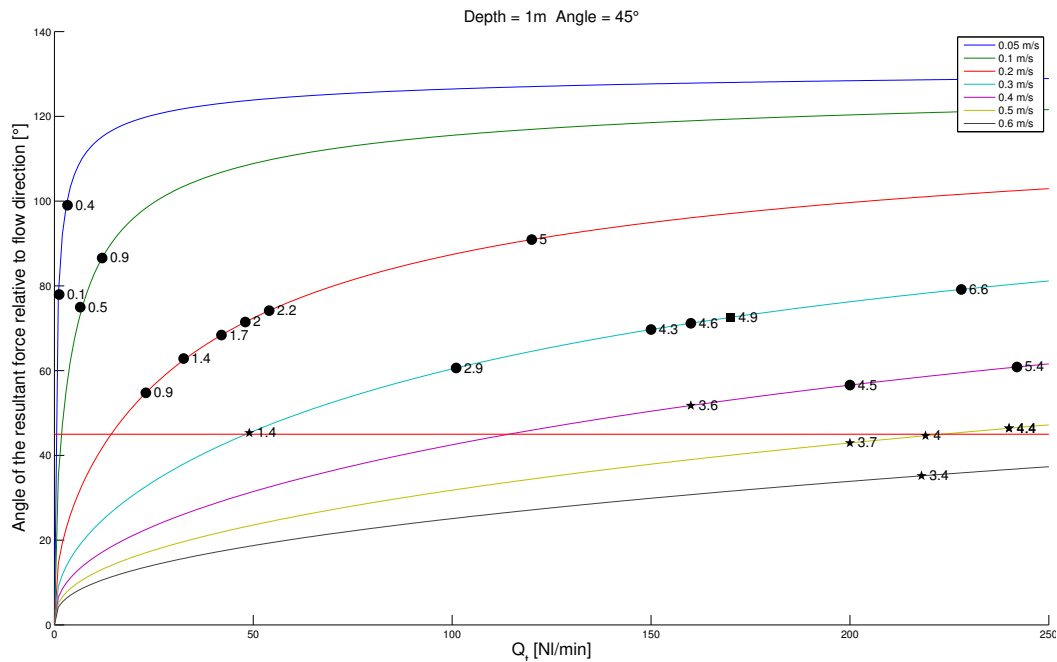
(b) 45° angle. Bulson

Figure 4.15: Direction of the resultant calculated with equation 4.3 (top) and Bulson's formula 4.4 (bottom). Points represent tested setups. A circle means that all foam chips and bottle caps were redirected into the corner. A square means that more than 90% of the foam chips and bottle caps were redirected. A pentagram means that less than 90% was redirected into the corner. The numbers next to the points represent the separation height calculated following formula 2.29.
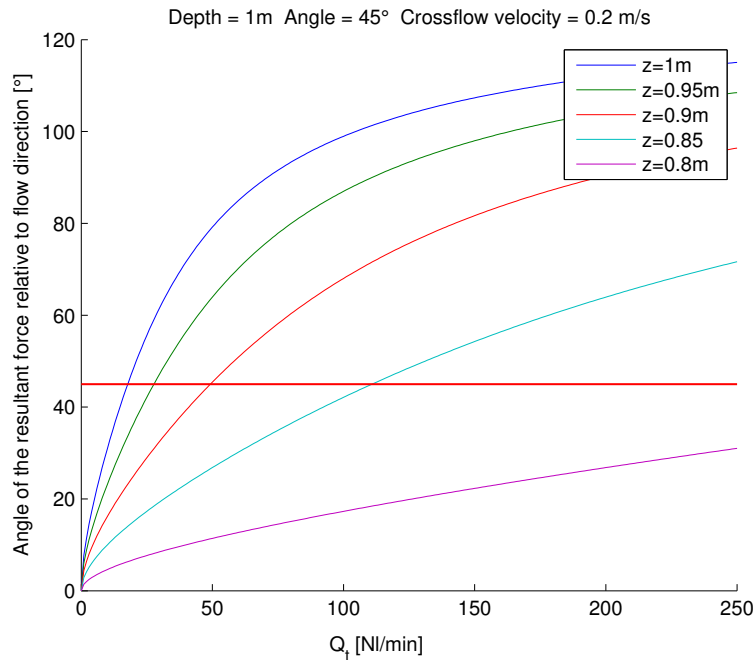
Figure 4.16: Angle of resultant at different depths. Total depth of the flume is 1 m; z = 0.95 m means that the resultant is calculated at a 5 cm depth.

Figure 4.17a shows the 45°angle with the resultant calculated at 3.5 cm depth with Bulson's formula. The dots represent only the foam chips and the bottle caps like in figure 4.15. In figure 4.17b the shapes represent also the other types of plastic from table 1.1 except the thin bags[6]; foam chips, bottle caps, balloons, partly filled bottles and six-pack wraps. It can be seen that airflows that were sufficient in order to redirect the foam chips and the bottle caps are not sufficient to redirect the deeper reaching types of plastic. For example at a crossflow of 0.2 m/s and an airflow of 23 Nl/min and 42 Nl/min. In order to get a better prediction of the required airflow to redirect also the other types of plastics the direction of the resultant needs to be determined at larger depths. Figure 4.17c shows this for a depth of 8 cm. The prediction seems to be accurate. For all other angles, the same figures for depths of 6, 8 and 10 cm can be found in appendix **??**. For the 63.4°angle the 10 cm version seems to give more accurate results. The same counts for the 26.6°angle. The predicted required airflow of the 10°angle seems to be insufficient again. This can still be caused by the very low separation height. It is interesting to see that the foam chips and bottle caps are only blocked when the prediction is made at depths larger than the depth they reach. While the other types of plastics are blocked when the depth around the centre of gravity (of the beer wraps) is taken. The beer wraps do, however, catch air sometimes, this might make them 'easier' to block. Also is the amount of repetitions is very little, therefore the predictions are not very substantiated.

---

[6]The thin bags are excluded because they are sometimes below the zone of influence of the bubble barrier and will, therefore, add some randomness to the results.

Table 4.7: Required airflow to keep the resultant upstream at a depth of 10 cm.

Angle	u_{cr}	[m/s]	0,05	0,1	0,2	0,3	0,4	0,5	0,6
10°	Q_t	[Nl/min]	1	2	5	14	31	60	103
	Q_t	[Nl/min/m]	0	0	1	2	5	10	17
	h_s	[m]	0	0,02	0,04	0,1	0,2	0,3	0,4
26.6°	Q_t	[Nl/min]	2	4	26	86	203	395	682
	Q_t	[Nl/min/m]	1	2	12	39	90,9	177	305
	h_s	[m]	0,09	0,1	0,7	1,6	2,9	4,6	6,8
45°	Q_t	[Nl/min]	2	9	64	213	505	984	1700
	Q_t	[Nl/min/m]	1	6	45	151	357	696	1202
	h_s	[m]	0,1	0,6	2,6	6,1	11,3	18,1	26,7
63.4°	Q_t	[Nl/min]	3	14	102	341	806	1574	2718
	Q_t	[Nl/min/m]	3	13	91	305	721	1407	2430
	h_s	[m]	0,4	1,3	5,3	12,4	22,8	36,7	54,0

Table 4.8: Required airflow to keep the resultant upstream at a depth of 10 cm. Separation height at least 0.5 m.

Angle	u_{cr}	[m/s]	0,05	0,1	0,2	0,3	0,4	0,5	0,6
10°	Q_t	[Nl/min]	16	28	41	72	92	112	131
	Q_t	[Nl/min/m]	3	5	9	13	16	19	23
	h_s	[m]	0,5	0,5	0,5	0,5	0,5	0,5	0,5
26.6°	Q_t	[Nl/min]	7	12	26	86	203	395	682
	Q_t	[Nl/min/m]	3	5	12	39	91	177	305
	h_s	[m]	0,5	0,5	0,6	1,6	2,9	4,6	6,8
45°	Q_t	[Nl/min]	8	9	64	213	505	984	1700
	Q_t	[Nl/min/m]	6	6	45	151	357	696	1202
	h_s	[m]	0,5	0,6	2,6	6,1	11,3	18,1	26,7
63.4°	Q_t	[Nl/min]	4	14	102	341	806	1574	2718
	Q_t	[Nl/min/m]	4	13	91	305	721	1407	2430
	h_s	[m]	0,5	1,2	5,3	12,4	22,8	36,7	53,9

The predicted required airflows at a depth of 10 cm are listed in table 4.7. The total airflow over the whole tube is given just like the airflow per meter of tubing. Also the separation height is calculated. It can be seen that the required total airflow is smaller when the angle is smaller even though the tube is longer. However, at small angles the separation height gets small. The experiments show that the separation height should be at least 0.5 m in order for the bubble barrier to work. In table 4.8 the required airflows are adjusted such that the separation height is at least 0.5 m.
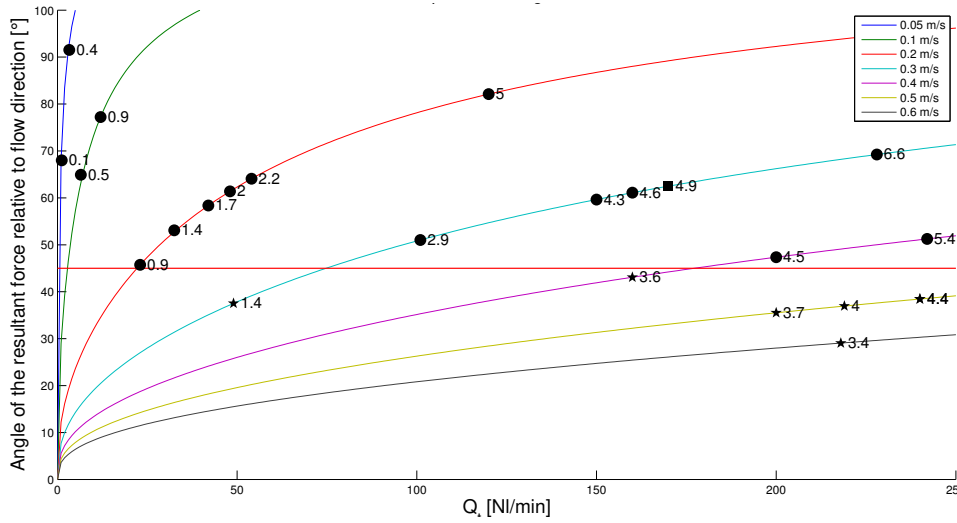
(a) ϕ=45° angle. Depth of 3.5 cm. Only foam chips and bottle caps represented in the shapes.
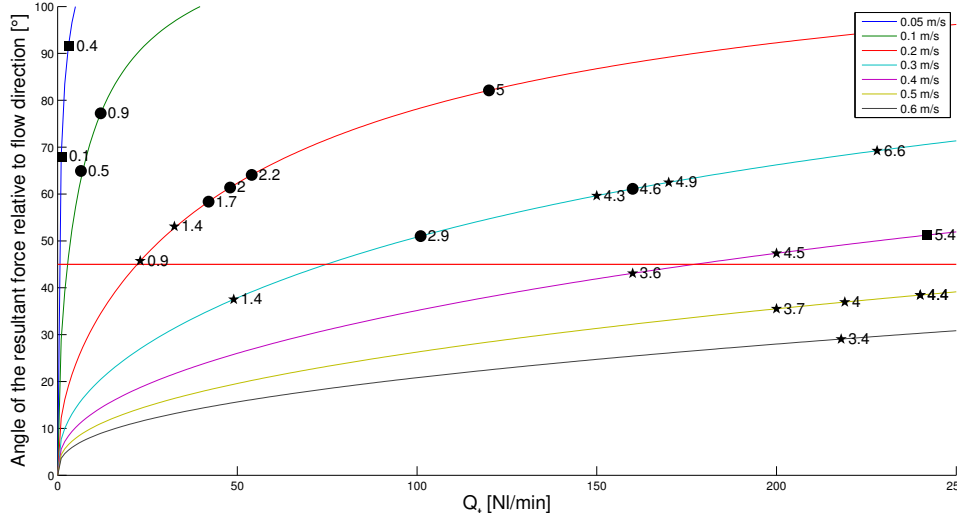
(b) ϕ=45° angle. Depth of 3.5 cm. Also balloons, bottles and beer wraps represented in the shapes.
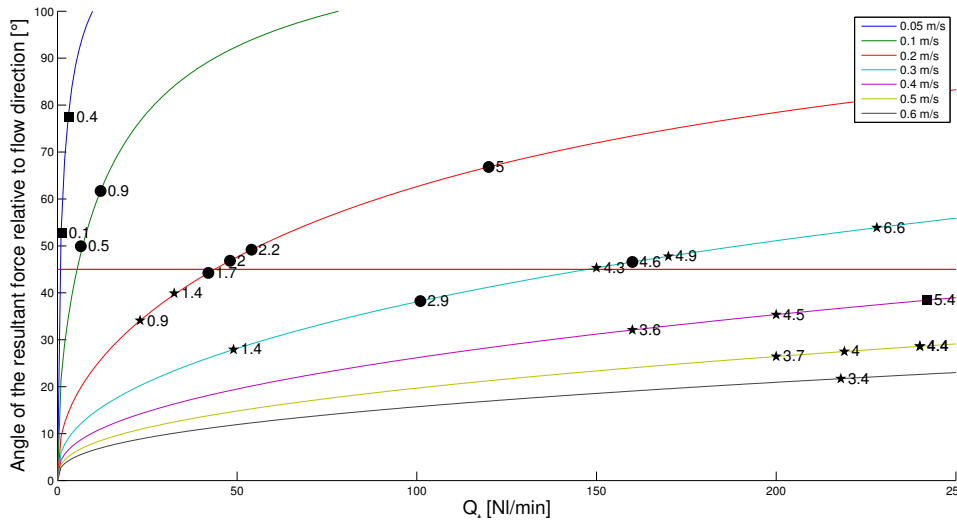
(c) ϕ=45° angle. Depth of 8 cm. Also balloons, bottles and beer wraps represented in the shapes.

Figure 4.17: Resultant of the velocities calculated for different depths.

4.4 Conclusion

In order to calculate the vertical centreline velocity of the rising plume two equations are available. When following equation 2.20 the spreading ratio and the location of the analytical origin need to be determined. The spreading ratio is found to be independent of the airflow. It increases linearly with crossflow velocity. The location of the analytical origin is taken as a constant value of 0.15 m. In the case of this flume, this calculation is shown to be sufficient with an error margin of 10% compared to when the empirically found values are taken. The calculated vertical velocities are corresponding very well to the observations. Equation 2.20 gives better results than Bulson's formula 2.7.

The vertical velocity of the plume together with the location in the x-direction between the tube and where the bubbles rise, make it possible to calculate the mean crossflow velocity over depth. Being sure about the crossflow velocity makes the predictions that are done on the working of the bubble barrier more substantiated.

To calculate the bubble-induced horizontal velocity also two equations are available. One is derived from the momentum balance, the other is again empirically found by Bulson. Knowing the crossflow velocity at height z as well as the direction and magnitude of the bubble-induced horizontal velocity at that height, the resulting flow direction can be determined. If the resulting flow remains on the upstream side of the line of rising bubbles the bubble curtain is assumed to redirect plastic particles at that height to the side. Bulson's formula gives a better agreement with the experimental results than the formula derived from the momentum balance. At a $10°$ angle, the suggested airflows are too small.

When the horizontal velocity induced by the bubbles is calculated with Bulson's formula, and the angle of the resultant of this velocity and the crossflow velocity both at a depth of 10 cm is calculated. The resulting required airflows are sufficient for angles ϕ of 63.4, 45 and $26.6°$. No guarantee can be given for the angles between these values since they have not been tested, but it is assumed that the same calculation will give adequate results. This method gives the safest results for the angles of $45°$ and $26.6°$. For high crossflow velocities this safety margin may lead to almost astronomical required airflows, therefore when $26.6°$ $<\phi<45°$ calculating the required airflow at a depth of 8 cm will suffice.

If separation height is lower than 0.5 meter the predictions do not give reliable results. The airflow should be increased until the separation height is 0.5 m. Based on the experiments performed it is impossible to say whether this threshold is at 0.5 m from the bottom of the flume, 0.5 m from the surface or at half the water depth. This makes predictions at larger water depths unreliable. Therefore it is advised at larger water depths to make sure that the separation height is not smaller than the water depth.

For a constant crossflow velocity, it can be seen that the smaller the angle of the tube the smaller the required total airflow Q_t. This total airflow is what is needed over the whole tube, so even though the tube is five times longer at a $10°$ as it is at a $62.4°$ angle. The $10°$ angle is in most cases not the optimal choice since the separation heights are very low and the predictions not accurate. Choosing a small angle drastically reduces the required airflow and therefore the energy consumption of the bubble barrier.

Chapter 5

Conclusion

This chapter consists of three sections. In the conclusion answers to the research questions are given. The discussion takes a closer look at the assumptions that are made during the research. Finally, the in the recommendations further research options are given.

5.1   Conclusion

The bubble barrier is a concept to filter plastics from rivers making use of a bubble curtain. This bubble curtain is realised by placing a perforated tube on the bottom of the river and pumping air through it. The rising bubbles enhance the surrounding water to flow upwards. At the surface, this vertical flow is transferred into a horizontal flow moving away from the bubble curtain on both sides. This horizontal flow in the surface layer is the main working principle of the bubble curtain in the function of a plastic barrier. Occasionally, a piece of plastic litter that is located in deeper layers catches air and rises to a depth where it can be blocked, this random phenomenon cannot be predicted. The focus of this study is on the development of a bubble barrier that blocks plastic debris floating in the surface layer.

The bubble-induced horizontal velocity is largest at the surface and decays linearly in depth down to 25% of the water column. Below this, the effect of the bubble curtain is negligible. The strength of the bubble-induced horizontal velocity also decays linearly in horizontal distance away from the screen up to four times the water depth away. The effect of the bubble curtain on the flow is maximum at the surface right upstream and downstream of the line of the rising bubbles.

Last century Bulson came up with empirical equations for the vertical centreline velocity of the plume and for the maximum bubble-induced horizontal velocity. Also, momentum balance derived equations are available for both velocities. Bubbles rise relative to the plume with a constant bubble slip velocity. Both theories are proposed for situations without a crossflow.

One of the hypotheses of this study is that a crossflow does not influence the vertical velocity of the plume and the bubble-induced horizontal velocity. Experiments are performed in the Easter Scheldt flume at Deltares to verify this hypothesis. The obtain the theoretical total flow field in the presence of a crossflow, the bubble-induced horizontal flow is added

to the crossflow at every point. The direction of the resulting flow at a certain point is determined by the summation of the crossflow velocity and the bubble-induced horizontal velocity at that point. The angle of the bubble curtain is, therefore, very important. Since the bubble-induced horizontal flow decreases linearly with depth, deeper in the water column the resulting flow is directed more in the direction of the crossflow. Plastic particles are assumed to follow the water by which they are surrounded. The direction of the resultant is, therefore, leading. If the resultant just upstream of the bubble curtain at a certain depth points to the upstream side of the line of rising bubbles, it is assumed that the plastic particles at that depth will stay at the upstream side too. When the bubble curtain is placed diagonally, they will be redirected to the side. If the resultant points to the downstream side the plastic particles are assumed to break through the bubble barrier. This theoretical prediction is compared with the experimental results.

In a river, the slope enhances the velocity of the flow. In the flume, the pump is responsible for this. The crossflow velocity has a logarithmic shape in depth. From the depth average crossflow velocity, the velocity at each depth can be determined. To check whether the crossflow velocity corresponds to the pump settings, the depth is divided by the mean rising time of the bubbles in the plume. The mean rising time can be observed from the experiments or calculated from the mean rising velocity of the bubbles in the plume. The bubbles in the plume rise with the speed of the water plus a constant bubble slip velocity of 0.25 m/s. The vertical velocity of the water in the plume has a Gaussian profile. At every depth between the initial region and the surface region, these profiles are similar with respect to the analytical origin. As previously mentioned, the vertical velocity at the centreline of the plume can be described by two equations. Both are compared with the experimental observations. Bulson's empirical formula predicts lower rising velocities than observed. For the formula obtained from the momentum balance, the location of the analytical origin and the spreading ratio are determined from experiments. These values are obtained experimentally and general solutions are presented. The resulting theoretical vertical velocities are in good agreement with the observed values.

The maximum horizontal velocity induced by the bubbles is also described by two equations, similar as the vertical velocity. Again the first one is empirically found by Bulson and the second one is derived from the momentum balance. These equations are based on a case without a crossflow. To examine the accuracy of both calculations in the presence of a crossflow the theoretical prediction of the working of the bubble barrier is compared with the experimental results. The empirical formula of Bulson gives more accurate results than the momentum balance derived equation. For all angles and crossflow velocities, the airflow required to keep the resultant upstream of the bubble curtain can be calculated at every depth. The airflow obtained at a depth of 10 cm is sufficient to block 90% of the tested objects in all experimental setups. A table is presented that shows the required airflow for different crossflow velocities and various angles of the tube. A smaller angle of the tube relative to the direction of the crossflow, logically, leads to a longer tube. However, the total required airflow to prevent plastics from passing gets smaller.

The ability of the bubble curtain to redirect plastics is used to check whether the theoretical velocities are not affected by the crossflow. Since many factors influence the working of the bubble barrier, it is not possible to say that the bubble-induced velocities are not affected at all. However, the experimental results show good agreement with the theoretical

predictions. Therefore, it can be concluded that the theory available for the case without a crossflow can be used to predict the required airflow needed to redirect plastics for all crossflows that are tested.

In the case of a high crossflow relative to the airflow, separation of the bubbles from the plume can occur. When separation occurs vertical momentum is lost. Therefore, the performance of the bubble barrier cannot be predicted. The height at which this occurs can be calculated. From the experiments is concluded that the separation height should be at least 0.5 m in order to have a working bubble barrier. Another table presenting the required airflows for different crossflow velocities and various angles taking the separation height into account is presented.

5.2 Discussion

Changes in temperature, which induce density differences, might be of influence for the effect of the bubble barrier. Since temperature gradients are very small over the length of the largest experiments (250m) these effects have not been taken into account. Density of water varies from 1000 kg/m^3 at 4°C to 998.2 kg/m^3 at 20°C. Since the water temperatures during the experiments performed for this researched are in the range between 8 and 12°C, the density has been assumed to be constant at 999.7 (10°C). Contamination is another possible cause of local density differences of water. Unfortunately, very little information is available on the contamination of rivers in the Netherlands. Therefore, in this study the influence on the density due to contamination is not taken into account. This assumption should not be problematic concerning the precision of the work.

Only a small number of repetitions have been tested for each type of plastic. More repetitions would have provided the possibility of statistical analysis and in particular estimations of confidence intervals.

The logarithmic river profile used for the flume is derived from wide river characteristics. The walls are not taken into account and the roughness is taken as a standard river. The flume is not a river and this might cause differences in the shape of the logarithmic profile. The friction of the walls might have caused the flow in the middle of the flume to be faster than in close to the walls. This is not measured at the experiments. If the flow in the middle was higher than assumed, in practice lower airflows are required than predicted. This makes the predicted airflows more conservative. At some setups, the effect of the walls was big as has been seen in section 4.3. This effect was most visible at large angles of the tube compared to the direction of the flow, since high airflows were required and the locations where the bubbles arose were not far apart in the x-direction. However, at smaller angles when a smaller airflow was required the walls did not seem to influence the result.

From the available empirical data, no relation between the airflow and the spreading ratio can be observed. It is, however, expected that the spreading increases when the airflow is drastically increased. A more substantiated relation could be found to define z_0 and c from the airflow and the crossflow velocity. This can be done by performing experiments at a 90° angle with changing air flows, crossflows and depths and only vary one parameter at a time.

5.3   Recommendations

The derived relation for c and z_0 should be checked for greater depths. It has been shown that the spreading of the bubbles is linear. This means that larger depths will lead to more spreading of the plume. The contained momentum will, however, remain constant. The question is whether the vertical momentum will still be translated into horizontal momentum. It should be further investigated whether Bulson's formula will still predict the required airflows accurately.

Furthermore, it should be determined whether the plastic particles are blocked when the resultant remains upstream at 10 cm below the surface or at 10% of the water depth below the surface.

The undulating motion of the plume can cause breakthroughs of the plastics. This effect is not taken into account in this research. With greater water depths the undulation of the plume increases in horizontal reach. This can lead to kinks in the line of rising bubbles. An abrupt change of the angle of the line of rising bubbles can be catastrophic.

Chapter 6

Bibliography

Abraham, G., van der Burgh, P., and de Vos, P. (1973). *Pneumatic Barriers to Reduce Salt Intrusion Through Locks*. Rijkswaterstaat.

Anderson, T. (2013). One World, One Ocean, One Mission. *Earth Common Journal*, pages 80–90.

Bulson, P. (1968). The Theory and Design of Bubble Breakwaters. In *Coastal Engineering*, pages 995–1015.

Co, T. (1970). Polymer Dictionary. Technical report.

Ditmars, K. and Cederwall, K. (1974). Analysis of Air-Bubble Plumes. In *Coastal Engineering*, pages 2209–2226.

Evans, J. (1955). Pneumatics and Similar Breakwaters. *Proceedings of the Royal Society of London A, Mathematical and Physical*, 231:457–466.

Fanneløp, T., Hirschberg, S., and Küffer, J. (1991). Surface Current and Recirculation Cells Generated by Bubble Curtains and Jets. *Journal of Fluid Mechanics*, 229:629–657.

GESAMP (2015). Sources, Fate and Effects of Microplastics in the Marine Environment: A Global Assessment. Technical report.

Hidalgo-Ruz, V., Gutow, L., Thompson, R. C., and Thiel, M. (2012). Microplastics in the Marine Environment: A Review of the Methods Used for Identification and Quantification. *Environmental Science Technology*, pages 3060–3076.

Hugi, C. (1993). *Modelluntersuchungen von Blasenstrahlen für die Seebelüftung*. PhD thesis, Institution für Hydromechanik und Wasserwirtschaft, ETH, Zurich.

Jordan, C. Midway. `http://www.chrisjordan.com/gallery/midway/#CF000478%2019x25`. Accessed: 22-02-2018.

Kobus, H. (1968). Analysis of the Flow Induced by Air-Bubble Systems. In *Coastal Engineering*, pages 1016–1031.

Lo, J. (1997). The Effect of Air-Bubble Barriers in Containing Oil-Slick Movement. *Ocean Engineering*, pages 645–663.

Milgram, J. (1983). Mean Flow in Round Bubble Plumes. *Journal of Fluid Mechanics*, 113:345–376.

MrTrashWheel. `http://baltimorewaterfront.com/healthy-harbor/water-wheel/`. Accessed: 24-02-2018.

PlasticsEurope (2016). Plastics the Facts 2016. Technical report.

PlasticSoupFoundation. `https://www.plasticsoupfoundation.org/`. Accessed: 24-02-2018.

PlasticSoupSurfer. `http://plasticsoupsurfer.org/`. Accessed: 24-02-2018.

PlasticWhale. `https://plasticwhalefoundation.com/`. Accessed: 24-02-2018.

Program, U. N. E. `http://web.unep.org/environmentassembly/estimated-8-million-tons-plastic-waste-enter-world%E2%80%99s-oceans-each-year-0`. Accessed: 22-02-2018.

Rezvani, M. (2016). *Bubble Plumes in Crossflow: Laboratory and Field Measurements of their Fluid Dynamic Properties with Application to Lake Aeration and Management.* PhD thesis, Texas AM University.

Riess, I. and Fanneløp, T. (1998). Recirculation Flow Generated by Line-Source Bubble Plumes. *Journal of Hydraulic Engineering*, 124:932–940.

Schmidt, W. (1941). Turbulente Ausbreitung eines Stromes Erhitzter Luft. *Zeitschrift für Angewandte Mathematik und Mechanik*, 265.

Simiano, M., Lakehal, D., Lance, M., and Yadigaroglu, G. (2009). Turbulent Transport Mechanisms in Oscillating Bubble Plumes. *Journal of Fluid Mechanics*, 633:119–231.

Socolofsky, S. and Adams, E. (2002). Multi-Pase Plumes in Uniform and Stratified Crossflow. *Journal of Hydraulic Research*, pages 661–672.

SurfriderFoundation. `https://www.surfrider.org/`. Accessed: 22-02-2018.

Taylor, G. (1955). The Action of a Surface Current Used as a Breakwater. *Proceedings of the Royal Society of London A, Mathematical and Physical*, 231:466–478.

TheOceanCleanup. `https://www.theoceancleanup.com/`. Accessed: 24-02-2018.

White, F. M. (2011). *Fluid Mechanics.* Mcgraw-Hill Education - Europe.